EWSR1::ETS-low cells promote metabolic reprogramming of the tryptophan-kynurenine-AHR axis, immunosuppression, and poor outcome in Ewing sarcoma

Martha J. Carreño-Gonzalez[1,2,3,4], Kimberley M. Hanssen[1,2,3], Ahmed Sadik[5], Alessa Henneberg[5], Anna C. Ehlers[1,2,3,4], A. Katharina Ceranski[1,2,3,4], Zuzanna A. Kolodynska[1,2,3,4], Malenka Zimmermann[1,2,3,4], Roland Imle[1,3,6], Florian H. Geyer[1,2,3,4], Alina Ritter[1,2,3,4], Ana Banito[1,3,6], Maximilian M. L. Knott[1,2,3], Shunya Ohmura[1,2,3], Florencia Cidre-Aranaz[1,2,3], Christiane A. Opitz[5], Thomas G. P. Grünewald[1,2,3,7]

1 Hopp Children's Cancer Center (KiTZ), Heidelberg, Germany
2 Division of Translational Pediatric Sarcoma Research, German Cancer Research Center (DKFZ), German Cancer Consortium (DKTK), Heidelberg, Germany
3 National Center for Tumor Diseases (NCT), NCT Heidelberg, a partnership between DKFZ and Heidelberg University Hospital, Germany
4 Medical Faculty, University of Heidelberg, Heidelberg, Germany
5 Division of Metabolic Crosstalk in Cancer, German Cancer Research Center (DKFZ), German Cancer Consortium (DKTK), Heidelberg, Germany
6 Soft-Tissue Sarcoma Junior Research Group, DKFZ, Heidelberg, Germany
7 Institute of Pathology, Heidelberg University Hospital, Heidelberg, Germany

Address for correspondence
Thomas G. P. Grünewald, MD, PhD
Division of Translational Pediatric Sarcoma Research
German Cancer Research Center (DKFZ)
Im Neuenheimer Feld 280
69120 Heidelberg, Germany
Tel 0049-6221-42-3718
Email t.gruenewald@dkfz-heidelberg.de

Article type	Research article
Word count	3,489 (excluding abstract, methods, references, and legends)
Display items	4 main figures, 1 supplementary figure, 1 supplementary table
Key words	Ewing sarcoma, AHR, Kynurenine, EWSR1::ETS, NK cells

ABSTRACT

How activational changes of driver oncogenes can promote metabolic reprogramming and cancer progression is largely uncharted territory. To address this issue, we employed Ewing sarcoma (EwS) as a model as it is driven by a single driver oncogene, namely chimeric EWSR1::ETS fusion transcription factors, whose fluctuating expression levels promote diverse transcriptional programs. While EWSR1::ETS-high cells display a rather sessile but proliferative phenotype and EWSR1::ETS-low cells are more invasive, the mechanisms underlying these different phenotypes remain poorly characterized. Here, using an integrative functional genomics approach, we show that low EWSR1::ETS fusion activity in patient tumors associates with poor outcome and increased signaling of the aryl hydrocarbon receptor (AHR). AHR signaling enrichment correlates with increased tumor infiltration by immunosuppressive cells and worse overall patient survival. Knockdown of EWSR1::ETS in EwS spheroid models cultured in human plasma-like media strongly alters tryptophan metabolism resulting in increased secretion of the AHR ligand kynurenine. Silencing of EWSR1::ETS reduced killing of EwS cells by natural killer (NK) cells, while AHR silencing increases NK cell-mediated killing. From a cell-intrinsic perspective, AHR knockdown inhibits proliferation, clonogenic, and spheroidal growth of EwS cells *in vitro*, which can be recapitulated by pharmacological AHR inhibition. Furthermore, *AHR* knockdown decreases tumor growth and metastasis *in vivo*. Collectively, our results illustrate how oncogene-mediated metabolic reprogramming of amino acid metabolism can translate into more aggressive disease phenotypes in cancer.

INTRODUCTION

Ewing sarcoma (EwS) is the second most common bone and soft tissue tumor in children, adolescents, and young adults (Grünewald *et al.*, 2018). Clinically, EwS is a highly aggressive malignancy, with 20–25% of patients presenting with metastases at diagnosis (Grünewald *et al.*, 2018; Cidre-Aranaz *et al.*, 2022). While 5-year survival rates are 70–80% for localized disease, disease recurrence occurs in a third of patients with initially localized disease and two-thirds of patients with metastatic initial disease, leading to survival rates of <30% (Stahl *et al.*, 2011; Grünewald *et al.*, 2018). It is therefore clear that improvement of EwS patient outcome requires novel treatment strategies which address causes of poor treatment response and metastasis, such as immune evasion (Grünewald *et al.*, 2020; Evdokimova *et al.*, 2023).

EwS tumors are driven by a single genetic event – a chromosomal translocation that results in the fusion of a *FET* family gene (*FUS*, *EWSR1*, *TAF15*) with an ETS family transcription factor (mainly *FLI1* or *ERG*). The resultant FET::ETS fusion oncoproteins, most commonly EWSR1::FLI1 (85% of cases) and EWSR1::ERG (10% of cases) (Delattre *et al.*, 1992, 1994; Sorensen *et al.*, 1994) act as aberrant transcription factors deregulating the cellular epigenome and transcriptome with tumorigenic implications (May *et al.*, 1993; Tomazou *et al.*, 2015; Orth *et al.*, 2022). Interestingly, there are recent reports of cell-to-cell fluctuations in the EWSR1::ETS fusion levels, where high EWSR1::ETS expression is associated with a more sessile but proliferative phenotype and low EWSR1::ETS expression with a more migratory and invasive phenotype and an enhanced ability to form metastases (Chaturvedi *et al.*, 2012, 2014; Wiles *et al.*, 2013; Franzetti *et al.*, 2017; Sannino *et al.*, 2017; Aynaud *et al.*, 2020).

EwS, like other sarcomas, has been shown to be immunologically ‘cold’, with few tumor infiltrating immune effector cells including T lymphocytes (Evdokimova *et al.*, 2023). While the degree of CD8 T cell infiltration and immunosuppressive macrophage infiltration has been found to negatively influence EwS patient outcome (Fujiwara *et al.*, 2011; Stahl *et al.*, 2011), immunotherapies, such as nivolumab, pembrolizumab, and cixutumumab, have thus far shown limited success in early clinical trials for EwS. A variety of factors has been attributed to these failures, including low immunogenicity of EwS tumors, MHC class I downregulation, presence of

immunosuppressive cells (MDSCs, M2-like tumor associated macrophages, regulatory T cells), and low infiltration of cytotoxic T and NK cells (Malempati *et al.*, 2012; Tawbi *et al.*, 2017; Davis *et al.*, 2020; Evdokimova *et al.*, 2023). Understanding the mechanism by which EwS tumors directly influence their local immune microenvironment and the potential role that fluctuating EWSR1::ETS fusion levels may play in maintaining an immunosuppressive state is therefore crucial to advance immunotherapeutic approaches.

Recent profiling studies have revealed that EWSR1::ETS fusions in EwS regulate the expression of many metabolism-related genes/proteins (Sen *et al.*, 2018; Issaq *et al.*, 2020; Orth *et al.*, 2022), including enzymes involved in the catabolism of tryptophan (Trp) via the kynurenine (Kyn) pathway (Mutz *et al.*, 2016). Metabolites generated from this pathway, such as Kyn and kynurenic acid (KynA), are known to activate the aryl hydrocarbon receptor (AHR) (DiNatale *et al.*, 2010; Opitz *et al.*, 2011), a ligand-activated transcription factor, which has recently emerged as a key regulator of anti-tumor immunity (Gutiérrez-Vázquez and Quintana, 2018; Rothhammer and Quintana, 2019; Opitz *et al.*, 2023). The functional significance of AHR activation for the EwS oncophenotype and the potential role of the Trp-Kyn-AHR axis in mediating the EwS immune environment, however, is unknown.

Here, we use an integrative functional genomics approach in EwS cell and mouse models to uncover the relevance and therapeutic potential of targeting the Trp-Kyn-AHR axis in EwS. We show that AHR signaling is strongly associated with poor outcome and immune infiltration scoring in EwS tumors and is upregulated upon induction of a low EWSR1::ETS expression state in EwS cells. Consistent with activation of AHR signaling in EWSR1::ETS-low cells, we observed significantly increased Kyn levels and found lowered sensitivity to killing by natural killer (NK) cells. Targeting of AHR restored NK cell-mediated killing of EwS cells, reduced EwS cell viability and clonogenicity *in vitro*, and nearly completely ablated EwS tumor growth *in vivo*. Thus, activation of AHR in EWSR1::ETS-low EwS cells may represent a targetable vulnerability that, when inhibited, can restore NK cell killing and halt tumor growth.

RESULTS

High AHR activity confers worse overall survival in EwS patients and correlates with EWSR1::ETS low activity

A prior study linked EWSR1::FLI1 with Trp and Kyn metabolism in EwS cell lines (Mutz *et al.*, 2016). However, it remains unclear whether this relationship holds true in EwS patient tumors, across EWSR1::ETS fusion types, or in cell models cultured under more physiological conditions, which better recapitulate human EwS tumors (Ceranski *et al.*, 2025). Hence, we first took advantage of a patient cohort with matched transcriptome data and clinical information (n=166 EwS patients) (Musa *et al.*, 2019). Assessment of the transcriptomic enrichment of an EWSR1::ETS activity score (Aynaud *et al.*, 2020) and subsequent K-means clustering across these patient tumors demonstrated that patients with low EWSR1::ETS activity had significantly shorter overall survival than those with high EWSR1::ETS activity (log-rank test; $P<0.0001$) (**Fig. 1a**). We then employed a newly defined pan-tissue AHR activity signature (Sadik *et al.*, 2020) comprising 166 genes (see Methods). As shown in **Figs. 1b,c**, consensus K-means clustering of the patients according to their AHR activity scores could identify two distinct clusters labeled K1 (AHR-low) and K2 (AHR-high). Next, we evaluated the association of newly defined AHR-clusters and showed that patients with high AHR scores (K2) had a significantly shorter overall survival than those with low AHR scores (K1) (log-rank test; $P=0.031$) (**Fig. 1d**). Consistent with AHR activity signature clustering, patients with high AHR scores (K2) exhibited significantly higher intratumoral expression levels of *AHR* and significantly altered mRNA expression levels of key enzymes (*IL4I1*, *TDO2*, *IDO1*, *KYAT1*) involved in Trp metabolism (**Figs. 1e,f**) indicating a metabolic shift toward increased Trp catabolism and production of the AHR ligand Kyn. Strikingly, assessing transcriptomic enrichment of an EWSR1::ETS activity score (Aynaud *et al.*, 2020) across these patient tumors and associating it with the previously calculated AHR scores showed a significant negative correlation between the two ($P=0.0006$, Fisher's exact test; relative risk = 0.64) (**Fig. 1g**). These effects observed in patients were mirrored *in vitro* in three-dimensional (3D) spheroids grown in human plasma-like medium (HPLMax) and reduced fetal calf serum (FCS) conditions (7%) in two EwS cell lines harboring doxycycline (DOX)-inducible shRNAs against their

respective fusions (EWSR1::FLI1 in MHH-ES-1 cells, EWSR1::ERG in TC-106 cells). As shown in **Fig. 1h**, silencing of either fusion for 96 h led to a significant deregulation of key enzymes in the Trp-Kyn pathway, including *TDO2*, *IL4I1*, and *KMO*. Specifically, *TDO2* (Kyn-synthesizing) was upregulated while *KMO* (Kyn-catabolizing) was downregulated. Consistent with this, we observed increased Kyn secretion in the supernatants (**Fig. 1i**). Levels of *AHR* itself were not robustly altered by EWSR1::ETS knockdown (data not shown), which is in line with observations that low EWSR1::ETS expression enhances AHR nucleus translocation rather than mRNA expression (Mutz *et al.*, 2016).

In sum, these data validate previous findings on EWSR1::FLI1 and Trp-Kyn metabolism and extend them to a clinically relevant phenotype in patient tumors with increased AHR signaling and enrichment in EWSR1::ETS-low cells.

High AHR activity correlates with higher infiltration of immune cells in EwS patients and contributes to an immunoprotective EwS phenotype *in vitro*

Since increased AHR activity has previously been linked to an immunosuppressive microenvironment that fostered tumor growth in other cancer types (Quintana *et al.*, 2008; Mezrich *et al.*, 2010; Liu *et al.*, 2018; Neamah, Nagarkatti and Nagarkatti, 2018; Greene *et al.*, 2019; Sadik *et al.*, 2020), we hypothesized that EwS tumors with increased AHR scores might exhibit an altered composition of the immune cell infiltrate. Interestingly, correlating computational Immune Pediatric Signature Scores (IPASS) (Mayoh *et al.*, 2023) inferred from our patient transcriptome data with the AHR scores revealed a significantly higher T cell infiltration of AHR-high EwS tumors (**Fig. 2a**). However, a more fine-grained analysis of the immune cell composition (see Methods) revealed not only an enrichment of B cells, (CD8+) T cells, and NK cells (**Fig. 2b**), but also a strong enrichment for immunosuppressive myeloid-derived suppressor cells (MDSCs) and regulatory T cells, increased presence of which have been observed in immunotherapy non-responders patients (Liu *et al.*, 2015; Oweida *et al.*, 2018; Weber *et al.*, 2018; Hou *et al.*, 2020; Petrova *et al.*, 2023; van Gulijk *et al.*, 2023) (**Fig. 2c**). This dual pattern may explain why the outcome of patients with AHR-high scores have worse outcomes despite displaying diverse immune infiltration overall.

Given that we observed increased Kyn secretion by EWSR1::ETS-low cells and that Kyn can inhibit surface expressed activating receptors (Chiesa *et al.*, 2006) and suppress the lytic function of NK cells (Trikha *et al.*, 2021), we tested whether EWSR1::ETS levels might influence NK cell activity against EwS cells. To this end, we carried out NK cell killing assays by co-culturing NK-92 cells with our EwS models with/without DOX-induced silencing of the respective EWSR1::ETS fusion. MHH-ES-1/TR/shEF1 and TC-106/TR/shERG cells were treated with or without DOX for 72 h then seeded at equal cell numbers for co-culture with NK-92 cells and subsequent viability normalized to their respective DOX controls to account for the influence of DOX. As shown in **Fig. 2d**, knockdown of EWSR1::ETS for 72 h significantly reduced NK cell-mediated killing of MHH-ES-1 and TC-106 EwS cells, even in spite of increased interferon-*γ* secretion – an activation marker of NK cells (Arase, Arase and Saito, 1996; Kaur, Celis and Jewett, 2025) – which was observed in MHH-ES-1 cells but not in TC-106 cells (**Fig. 2e**). To test the possibility that this effect of EWSR1::ETS-low expression on NK cell killing is meditated via AHR signaling in EwS cells, we generated single-cell cloned DOX-inducible shAHR EwS cells, which exhibited a strong and comparable knockdown of AHR at the mRNA and protein levels across all models (**Figs. 2f,g**). As above, MHH-ES-1/TR/shAHR255 cells (bulk and single clones) were treated with or without DOX for 72 h prior to being seeded at equal numbers and co-cultured with NK cells for a further 24 h. Excitingly, this revealed a strong enhancement of NK cell-mediated killing upon AHR silencing (**Fig. 2h**), which had a comparable magnitude (~2-fold) to the inhibitory effect of the EWSR1::ETS knockdown. Collectively, these *in situ* and *in vitro* analyses suggest that AHR activation accounts, at least in part, for the immunoprotective phenotype observed in EWSR1::ETS-low cells.

AHR promotes proliferation and clonogenicity of EwS cells *in vitro*

Since our results pointed to a role of EWSR1::ETS-mediated metabolic reprogramming of EwS cells concerning Trp-Kyn metabolism in cell-extrinsic phenotypes, we wondered whether this may also have cell-intrinsic effects. To test this possibility, we subjected our single cell-cloned shAHR EwS models to a series of *in vitro* assays in physiological medium (HPLMax) (Cantor *et al.*, 2017; Vande Voorde *et al.*, 2019; Ceranski *et al.*, 2025). As shown in **Fig. 3a**, conditional AHR silencing

significantly reduced proliferation of MHH-ES-1 cells in short-term assays (96 h), which was accompanied by a delay in cell cycle progression at G1 in MHH-ES-1 and TC-106 cells (**Fig. 3b**). To assess the cell-intrinsic effects of AHR for a longer period of time (10–12 days), we carried out colony-formation assays. Strikingly, knockdown of AHR almost completely suppressed clonogenic growth of both EwS cell lines (**Fig. 3c**), an effect not observed for control cells expressing a DOX-inducible non-targeting shRNA (**Supplementary Fig. 1a**). Given these strong effects and to exclude a potential bias through clonal artefacts, we repeated key assays with the parental bulk-level shAHR cells, which exhibited similar remaining AHR levels upon DOX-treatment, and comparable phenotypes regarding cell proliferation and clonogenicity as well as spheroidal growth (**Supplementary Figs. 1b–e**). To examine whether similar effects could be achieved via pharmacological inhibition and to explore the potential of AHR as a drug target in EwS, we subjected MHH-ES-1 and TC-106 cells to ascending doses of the specific small molecule AHR antagonist GNF-351 (Smith *et al.*, 2011; Van Den Bogaard *et al.*, 2015) and carried out short-term viability and long-term colony formation assays, which recapitulated our AHR knockdown results (**Figs. 3d,e**). Taken together, these results point to an important role of AHR as a druggable target promoting proliferation of EwS cells *in vitro*.

AHR promotes tumor growth and metastasis of EwS *in vivo*

Given the strong phenotypes observed upon AHR silencing in our *in vitro* models grown in physiological conditions, we next tested the impact of AHR on tumor growth and metastasis *in vivo*. To that end, we inoculated our single cell-cloned shAHR EwS cells subcutaneously into the right flank of NOD/Scid/gamma (NSG) mice and started DOX-treatment once tumors were palpable. As shown in **Fig. 4a**, conditional knockdown of AHR led to tumor regression in both MHH-ES-1 and TC-106 cells. In a next step, we employed a spontaneously metastasizing orthotopic model by inoculating MHH-ES-1/TR/shAHR cells into the tibial plateau of NSG mice and started DOX-treatment the subsequent day. Mice were killed at individual days once predefined humane endpoints, such as signs of tumor-associated limping of the injected leg or abdominal extension as a possible sign of metastasis, were detectable. At the endpoint, there was

a significant reduction in the weight of the primary tumors of the *AHR*-silenced DOX+ group, as determined by surrogate measure of the weight of the inoculated leg (**Fig. 4b**). Further, necropsy of the animals showed that while macroscopically there were no metastases in organs other than liver, there was a significant difference in liver weights concordant with the significantly reduced number of macroscopically detectable liver metastases in the AHR knockdown group (DOX+; **Figs. 4c,d**). Collectively, these *in vivo* results further emphasize the important role of AHR signaling for tumor progression of EwS.

DISCUSSION

EwS is an aggressive pediatric cancer with frequent early metastasis and high rates of relapse. While novel immunotherapies have seen improvement in patient outcomes for other difficult to treat cancers, EwS has shown poor responses in early clinical trials for immunotherapies, largely due to their immunologically cold nature. While metabolic crosstalk in the tumor microenvironment regulates immunogenicity, there is very little known about how metabolic regulation by the EwS driver fusion may influence anti-tumor immunity.

Trp metabolism via the Kyn pathway has gained attention in past years given the direct connection of its downstream metabolites (Kyn, KynA) to AHR activation, tumor progression, and immunosuppression in glioblastoma, and breast, liver, and non-small cell lung cancers (Opitz *et al.*, 2011; Ye *et al.*, 2018; Solvay *et al.*, 2023; Holfelder *et al.*, 2024). Increased AHR nuclear translocation upon silencing of EWSR1::FLI1 in EwS cell lines had previously established a role of this fusion as a repressor of AHR activity (Mutz *et al.*, 2016). Here, we show for the first time that EwS patients with higher AHR activity have worse overall survival and increased infiltration signatures for activated innate and adaptive immune cells as well as important immunosuppressive cells (MDSCs and regulatory T cells). As high AHR activity EwS tumors were found to have increased signatures for activated B and T cells and CD56dim NK cells, further investigation of how AHR activity in EwS influences the activation and function of immune cells is warranted. Indeed, we observed reduced killing of EWSR1::ETS-low cells by NK-92 cells despite

increased interferon-γ levels in the co-culture. Whether this effect is driven by reduced function of the NK cells, intrinsic resistance of the EWSR1::ETS-low cells to NK cell killing, or a combination of both is unclear. While it has been established that Kyn has a direct negative impact on NK cell function (Chiesa *et al.*, 2006; Trikha *et al.*, 2021), induction of potential immunoprotective mechanisms upon low EWSR1::ETS expression is less well understood. Several immune evasive mechanisms have been identified on EwS tumor cells, such as high cell surface expression of phagocytic inhibitory signals such as CD47 overexpression and downregulation of pro-phagocytic signals such as cell surface calreticulin (Luo *et al.*, 2024), and upregulation of non-classical HLA types such as HLA-E or HLA-G (Spurny *et al.*, 2017; Altvater *et al.*, 2021), but these have not been studied in the context of fluctuating EWSR1::ETS levels. The present study is therefore significant in establishing a link between EWSR1::FLI1 as well as EWSR1::ERG expression, AHR activation, and reduced NK cell killing, though the precise molecular mechanisms remain to be fully elucidated. Characterization of cell surface markers expressed on both immune and EwS cells will be important to better understand the mechanism by which EWSR1::ETS-low EwS cells evade NK cell-mediated cytotoxicity. It should be noted that, while NK-92 cells are widely used as adequate models for NK cell studies (Klingemann, 2023) , future studies in the EwS context should also include and test non-transformed primary NK cells as well as other cytotoxic immune cells.

Further to its role in mediating immune evasion of EWSR1::ETS-low EwS cells, we also demonstrated that AHR signaling is important for proliferation, clonogenicity, and cell cycle progression of EwS cells. Importantly, we showed that AHR silencing in subcutaneous EwS xenografts induced tumor regression and in orthotopic models significantly reduces liver metastases. This is consistent with studies of other cancers types where high AHR activation promoted cell proliferation, tumor formation, and tissue invasion (Puga, Xia and Elferink, 2002; Peng *et al.*, 2009; Murray, Patterson and Perdew, 2014; Stanford *et al.*, 2016). While these pro-tumorigenic effects of AHR have been linked to reduced cell-to-cell contact by downregulation of E-cadherin and increased cell motility and survival (Dietrich and Kaina, 2010; Opitz *et al.*, 2011; D'Amato *et al.*, 2015; Novikov *et al.*, 2016; Shadboorestan *et al.*, 2019), further experiments will be needed to clarify which of these pro-tumorigenic mechanisms may underly the effect of AHR

silencing observed on EwS metastasis and tumor regression. Additionally, as there is a present lack of immunocompetent EwS mouse models, the establishment of humanized mouse models for EwS will also be important to test the effect of *AHR* knockdown on anti-tumor surveillance *in vivo*.

Given the pro-tumorigenic effects of AHR in EwS cells and the immune evasion afforded to EWSR1::ETS-low cells, our findings support the Trp-Kyn-AHR axis as an important potential therapeutic target for EwS. Pharmacological inhibitors of upstream Trp-Kyn pathway enzymes as well as direct AHR inhibitors are currently under evaluation at different stages of *in vitro*, preclinical, and clinical investigation. TDO2 and IL4I1 contribute to the synthesis of AHR agonists, namely Kyn and indole metabolites (I3A, IAA, ILA) respectively (Platten *et al.*, 2019; Sadik *et al.*, 2020; Opitz *et al.*, 2023). As the expression of both enzymes was elevated upon knockdown of the EWSR1::ETS fusion, it will be important to test whether direct targeting of TDO2 and IL4I1 can adequately reduce AHR activation in EWSR1::ETS-low cells. Few selective and potent inhibitors, however, have been described for TDO2, none of which have progressed to clinical trial (Kozlova and and Frédérick, 2019) and some additionally act as AHR agonists and are therefore of limited use in this context (Opitz *et al.*, 2020). The link between activation of AHR by metabolites produced downstream of IL4I1 and tumor cell immune evasion has only recently been recognized (Sadik *et al.*, 2020), and inhibitors are therefore still in an early stage of development (MacKinnon *et al.*, 2020; Hess *et al.*, 2025). IDO1, like TDO2, synthesizes a precursor to Kyn, and was found to be more highly expressed in EwS patients with a high AHR activity score. While several IDO1 inhibitors such as epacadostat and navoximod have been investigated in combination with PD-1/PD-L1 targeting therapies, these failed to demonstrate clinical benefit in trials for metastatic melanoma (Long *et al.*, 2019) or advanced solid tumors (Jung *et al.*, 2019), likely due to structural resemble of the IDO1 inhibitor to AHR agonists (Lewis *et al.*, 2017; Moyer *et al.*, 2017; Long *et al.*, 2019).

In light of this, and given that we found that the direct small molecule AHR inhibitor GNF-351 recapitulated the anti-proliferative phenotype observed with genetic silencing of AHR in EwS, direct targeting of AHR may be the most effective strategy for this pathway in EwS. Efforts are

underway to develop selective AHR inhibitors, including AHR modulating compounds that fine-tune rather than fully antagonize AHR activity to limit potential systemic effects (Yin *et al.*, 2012; Kober *et al.*, 2023; Aggen *et al.*, 2024). Preclinical testing of GNF-351 or other such antagonists or selective modulators of AHR in *in vivo* xenograft models will shed light on the translational potential of this approach for EwS.

This study illustrates the interconnection of EWSR1::ETS fusion oncogenes, the Trp-Kyn pathway, and AHR activation in EwS *in situ* and *in vivo*. We found that AHR activity drives proliferation of EwS cells while mediating NK cell resistance and possible immune evasion of EWSR1::ETS-low cells. Silencing of AHR *in vivo* regressed EwS tumor growth while strongly suppressing metastasis. This work deepens our understanding of how the EwS driver fusion can regulate cellular metabolism to manipulate local immune responses and highlights the Trp-Kyn-AHR axis as a novel therapeutic target to improve treatment options for EwS, particularly for metastatic disease.

CONFLICT OF INTEREST

Authors of this manuscript have patents on AHR inhibitors in cancer (WO2013034685, C.A.O.); A method to multiplex tryptophan and its metabolites (WO2017072368, C.A.O.); A transcriptional signature to determine AHR activity (WO2020208190, A.S., C.A.O.); Interleukin-4-induced gene (IL4I1) and its metabolites as biomarkers for cancer (WO2021116357, A.S., C.A.O.). The other authors declare no conflict of interest.

AUTHOR CONTRIBUTIONS

M.J.C.G. carried out the majority of the *in vitro* and *in vivo* experiments. K.M.H, A.K.C., F.H.G., Z.A.K., M.Z. and A.R. helped in molecular cloning and *in vitro* assays. S.O. helped in NK-cell experiments and R.I., A.B., and F.C.A. in *in vivo* experiments. A.S. and A.C.E. carried out bioinformatics analyses. A.H. and M.J.C.G. carried out measurements of Kyn levels. M.M.L.K. and

C.A.O. provided experimental guidance. M.J.C.G., K.M.H. and T.G.P.G. wrote the paper and designed the figures. T.G.P.G. conceived and supervised the study and provided laboratory infrastructure. All authors read and approved the final manuscript.

ACKNOWLEDGEMENTS

We thank S. Kutschmann, F. Zahnow, N. Gmelin, and S. Knoth for excellent technical assistance. We also thank Prof. Dr. A. Cerwenka and Dr. A. Stojanovic (Department of Immunobiochemistry, Mannheim Institute for Innate Immunoscience, Medizinische Fakultät Mannheim der Universität Heidelberg, Germany) for consultations regarding NK cell experiments.

FUNDING

This work was mainly supported by grants from the Boehringer-Ingelheim foundation, the German Cancer Consortium (DKTK, PredictAHR) and the German Cancer Aid (DKH-70115315). The laboratory of T.G.P.G. is supported by grants from the Matthias-Lackas foundation, the Dr. Leopold und Carmen Ellinger foundation, Dr. Rolf M. Schwiete foundation (2021-007; 2022-031), the German Cancer Aid (DKH-70114278, DKH-70115914), the SMARCB1 association, the Ministry of Education and Research (BMBF; SMART-CARE and HEROES-AYA), the KiKa foundation, the Fight Kids Cancer foundation (FKC-NEWtargets), the KiTZ-Foundation in memory of Kirstin Diehl, the KiTZ-PMC twinning program, Sarcoma Research UK, and the Barbara and Wilfried Mohr foundation. The laboratory of T.G.P.G. is co-funded by the European Union (ERC, CANCER-HARAKIRI, 101122595). Views and opinions expressed are however those of the authors only and do not necessarily reflect those of the European Union or the European Research Council (ERC). Neither the European Union nor the granting authority can be held responsible for them. A.R., F.H.G., and A.C.E. were supported by scholarships of the German Cancer Aid and the German Academic Scholarship Foundation. M.Z. also acknowledges funding by the German Academic Scholarship Foundation as well as by the Kind-Philipp foundation. K.M.H. was

supported by a fellowship of the Alexander von Humboldt foundation. C.A.O. acknowledges support from the ERC under the European Union's Horizon 2020 research and innovation programme (grant agreement number 101045257, CancAHR).

METHODS

Cell lines and cell culture conditions

Human HEK293T, MHH-ES-1, and NK-92 cell lines were provided by the German collection of Microorganisms and Cell cultures (DSMZ). The human EwS cell line TC-106 was kindly provided by the Children's Oncology Group (COG). The standard cell culture conditions for HEK293T cells and EwS cells for viral transduction were as follows: RPMI 1640 with stable glutamine (ThermoFisher Scientific, USA), 10% tested doxycycline (DOX)-free FCS, penicillin (100 U/mL), and streptomycin (100 µg/mL) (1% penicillin/streptomycin) (Sigma-Aldrich, Germany). Newly established physiological conditions that better recapitulate the *in situ* situation were used for performing all other EwS experiments using HPLM (ThermoFisher Scientific, USA) plus unique Plasmax components, 7% FCS, and 1% penicillin/streptomycin (Ceranski *et al.*, 2025).

To culture the NK-92 cell line, the base medium was composed of RPMI 1640 medium with 2 mM L-glutamine, heat-inactivated FCS (56 ºC for 30 min), and 1% penicillin/streptomycin. Lyophilized IL-2 was resuspended in 50 µL 100 mM acetic acid and 50 µL of 0.2% FCS in PBS (10^6 U/mL) and stored at −80 ºC until use. The daily cell culture media was prepared by combining 50 mL of the base medium with 500 µL of HEPES 1 M (final concentration 10 mM) and 5 µL IL-2 (final concentration 10 ng/mL). NK-92 cells were maintained at confluency of 100,000–400,000 cells/mL.

All cell lines were incubated at 37ºC and 5% CO_2 in a controlled humidified environment. All cell cultures were regularly tested for mycoplasma contamination (Mycoplasma PCR Detection Kit, Applied Biological Materials) and identified by SNP (single nucleotide polymorphism) or STR (short tandem repeat)-profiling (Multiplexion, Heidelberg, Germany).

Survival analysis of EwS patient cohort and AHR signaling and specific type of immune cell infiltration analysis

The microarray data of 166 EwS tumors of the following datasets GSE63157, GSE34620, GSE12102, GSE17618 (Scotlandi *et al.*, 2009; Savola *et al.*, 2011; Postel-Vinay *et al.*, 2012; Volchenboum *et al.*, 2015) were downloaded from the Gene Expression Omnibus database (https://www.ncbi.nlm.nih.gov/geo/). The datasets generated on the Affymetrix Human Exon 1.0 ST Array were preprocessed and normalized using the *AffyGEx* package (https://github.com/ahmedasadik/AffyGEx). Datasets generated on the Affymetrix Human Genome U133 Plus 2.0 Array were processed and normalized using *affy* (Gautier *et al.*, 2004) and *gcrma* (Irizarry *et al.*, 2003). The normalized expression matrices were z-transformed and merged into a single expression matrix and batch corrected using principle component analysis and the *removeBatchEffect* function from *limma* (Ritchie *et al.*, 2015). The batch corrected matrix was used to calculate a single sample AHR activity score as described previously (Sadik *et al.*, 2020), in addition to performing weighted gene co-expression network analysis (WGCNA) (Langfelder and Horvath, 2008). To identify WGCNA modules that associate with AHR activity, we correlated the WGCNA modules with the AHR activity scores, and performed a global test using the WGCNA modules as predictors of the AHR activity score. Module selection was set at a Pearson correlation coefficient threshold of ± 0.2 at a *P*-value of 0.05 (Evans, 1996), and at a *P*-value of 0.05 for the global test (AHR associated modules, AAMs). K-means consensus clustering (Wilkerson and Hayes, 2010) was performed using the AAMs to identify the number of clusters. The Kaplan-Meier method and log-rank test were used to evaluate the association of the EwS AHR clusters with survival outcome (Therneau and Grambsch, 2000; Therneau, 2024). Single sample immune infiltration scores were generated using MCP-counter, and by applying GSVA (Hänzelmann, Castelo and Guinney, 2013) to the immune signatures (Charoentong *et al.*, 2017). The Wilcoxon rank sum test was used for all pairwise group comparisons.

Single-sample gene set enrichment analysis (ssGSEA)

To quantify sample-based transcriptomic signature enrichment in the EwS patient cohort (n=166) single sample gene-set enrichment analysis (ssGSEA) was employed (Barbie *et al.*, 2009; Hänzelmann, Castelo and Guinney, 2013). EWSR1::ETS fusion activity signature was assessed using the IC-EwS gene signature previously established (Aynaud *et al.*, 2020). The resulting ssGSEA scores were used to classify tumor samples into EWSR1::ETS-high and EWSR1::ETS-low groups via K-means clustering. Similarly, T-cell infiltration levels were inferred using the Immune Pediatric Signature Score (IPASS), a validated 15-gene immune signature associated with CD8+ T-cell infiltration in high-risk pediatric tumors (Mayoh *et al.*, 2023). Resulting immune infiltration scores were subsequently used to classify tumors into T cell infiltration-high and T cell infiltration-low groups. To examine potential relationships between AHR pathway activation, EWSR1::ETS fusion activity, and immune cell infiltration 2×2 contingency table with two-tailed Fisher's exact tests were employed.

Spheroidal growth for 3D assays

EwS spheres were grown on high gel-strength agar coated T-25 flasks as previously described (Ceranski *et al.*, 2025). For MHH-ES-1/TR/shEF1 1,800,000 cells per T-25 were seeded and for TC-106/TR/shERG, 800,000 cells per T-25. Spheroids were treated with 1 µg/mL DOX for 96 h, with DOX refreshed every 48 h, then spheroids collected for RNA isolation or the supernatant collected for Kyn level measurement.

RNA isolation, reverse transcription, and qRT-PCR

To determine knockdown efficiency and gene expression after treating cells with DOX, RNA isolation was performed using the NucleoSpin® RNA kit as per manufacturer's instructions (Macherey-Nagel, Germany), followed by cDNA synthesis using 1,000 ng/µL or 500 ng/µL RNA with the High-Capacity cDNA Reverse Transcription Kit (Applied Biosystems, USA) as per manufacturer's instructions. qRT-PCR reactions were performed using SYBR Select master mix (Applied Biosystems, USA) with 1:5 diluted cDNA and 0.5 µM forward and reverse primers

adjusted to a reaction with total volume of 15 μL. Reactions were performed on a CFX Opus 96 (Bio-Rad, USA) and analyzed using Bio-Rad CFX Maestro 2.3 version software. Gene expression was normalized to the *RPLP0* housekeeping gene and fold change calculated by the $2^{-\Delta\Delta}$CT method (Livak and Schmittgen, 2001). Oligonucleotides and primers were purchased from Eurofins genomics (Sigma-Aldrich) and are listed in **Supplementary Table 1**. The thermal conditions for qRT-PCR were as follows: heat activation at 95 ºC for 2 min (1 cycle), DNA denaturation at 95 ºC for 10 sec, and annealing and extension at 60 ºC for 10 sec (total 50 cycles). Final denaturation at 95 ºC for 30 sec, annealing at 65 ºC for 30 sec, and extension at 65–95 ºC (increase 0.5 ºC/5 sec) 1 cycle.

Ultra-High-Performance Liquid Chromatography to measure Kyn

Kyn levels were measured in the supernatant of EwS cells in EWSR1::ETS-high and -low context, in the established physiological conditions (3D, HPLMax, 7% FCS, 1% penicillin/streptomycin). DOX treatment was performed for 96 h, and refreshed every 48 h. Cells were grown in spheres as described before. In summary, spheres and supernatant were collected in 15 mL reaction tubes and centrifuged for 4 min, 1,200 rpm, room temperature. A record of the total volume of each sample was taken for normalization. 200 μL of supernatant were collected in reaction tubes and snap frozen in liquid nitrogen immediately. The rest of the supernatant was discarded, and spheres were further collected for protein quantification. Spheres were lysed in RIPA buffer (Serva electrophoresis, Germany) for 10 min and protein was quantified with Pierce BCA Protein Assay Kit (ThermoFisher Scientific, USA). Supernatant was stored in –80 ºC until further analysis. For the sample preparation for Kyn measurement, 33.73 μL of trichloroacetic acid was added to 200 μL of each sample, vortexed to mix, and incubated for 15 min. After, samples were centrifuged at 4 ºC, 15,000 g for 10 min and supernatant transferred to 250 μL conical point glass inserts for UHPLC (Agilent Technologies, USA). Measurements were performed in an UltiMate 3000 UHPLC (ThermoFisher Scientific). Metabolites were separated by reversed-phase chromatography on an Accucore™ aQ C18 column (ThermoFisher Scientific) 2.6 µm, 2.1 × 150 mm heated to 35 °C and equilibrated with five column volumes of 98% solvent A (H_2O with 0.1% trifluoroacetic acid) with a

flow rate of 0.55 mL/min. Separation of Trp and Kyn was achieved by increasing concentration of solvent B (acetonitrile with 0.1% trifluoroacetic acid) in solvent A with the following gradient: 4 min 0% B, 10 min 5% B, 13 min 15% B, 13.01 min 20% B until min 15, returning back to 0% at 15.01 min until 18 min. Levels of Kyn were measured at 365 nm absorbance and data analysis was performed with the software Chromeleon v7.2 (ThermoFisher Scientific).

NK-92 killing assays

To evaluate the killing effect of NK-92 cells against EwS cells, a co-culture was performed and cell viability was evaluated. First, EwS cells (with DOX-inducible knockdown of *EWSR1::ETS* or *AHR*) were pre-treated with DOX for 72 h (DOX refreshed after 48 h). After 72 h, EwS cells were seeded in 12-well plates at equal cell numbers for both DOX conditions and left to attach for 4 h. NK-92 cells were then added at a 1:1 ratio to the EwS cells and co-cultured for 24 h. For readout, medium was removed and cells were washed twice with PBS to remove the NK-92 cells. Fresh EwS medium was added and cell viability was determined via resazurin assay as described below.

Resazurin assay

Resazurin assays were performed to determine cell viability in the drug-response assays following treatment with AHR inhibitors and after co-culture with NK-92 cells. The protocol was followed from already published resazurin colorimetry protocol (Musa and Cidre-Aranaz, 2021) and adapted the volumes accordingly. Resazurin (Sigma-Aldrich, Germany; 1 g/L in PBS) stock solution was diluted 1:10 in PBS to a working stock solution before the assay readout. For NK-92 co-culture experiments, 200 µL resazurin was added to wells containing 500 µL media. For drug response assays, 50 µL resazurin was added to wells containing 200 µL media. Following resazurin addition, plates were incubated for 5 h at 37 ºC, and fluorescence readout was performed in the microplate reader GloMax®-Multi Detection System (Promega, USA) with a 560 nm excitation–590 emission filter. Wells without seeded cells (only medium) were use for background subtraction.

Interferon-γ measurement after EwS and NK-92 co-culture

Similar to the NK-92 killing assay, EwS cell lines were first DOX treated to knockdown the respective *EWSR1::ETS* fusion for 72 h. In this case, EwS cells were seeded in a 96-well white plate (clear bottom with lid) for luminescence readout (MHH-ES-1/TR/shEF1, 20,000 cells/well). After 4 h, NK-92 cells were added in a 1:1 ratio and co-cultured for 24 h. In addition, NK-92 cells were seeded only (16,000 cells per well) to subtract the amount of interferon-γ these cells produce alone. After 24 h co-culture, the Lumit™ interferon-γ Human Immunoassays (Promega, USA) was followed as indicated by the manufacturer's protocol. Luminescence was measured in a plate reader and interferon-γ levels were calculated relative to the control.

***AHR* knockdown establishment with pLKO Tet-On construct**

AHR silencing (transcript ID: Human NM_001621.5) was achieved by cloning the shRNA oligonucleotide sequences into the Tet-pLKO-puro backbone (Addgene #21915, USA). Design of the shRNA sequences were obtained from the database GPP Web Portal. Different criteria for selection were followed: Match position (CDS [coding sequence], 3'UTR [untranslated region]), intrinsic score (<10) and Specificity-Defining Region (SDR) Match (100%). In addition, five shRNA sequences were obtained from the online tool SplashRNA (Pelossof *et al.*, 2017). Sequences with a Splash score of 1.5 or higher were selected. The selected sequences were adapted to the Tet-pLKO-puro vector by adding compatible restriction site overhangs of the EcoRI and AgeI enzymes (New England Biolabs, Germany), loop sequence and termination sequence. Details of the cloning protocol including bacteria transformation, single bacteria colony screening, lentivirus production and antibiotic selection has been already established previously by us (Musa, 2021; Orth *et al.*, 2022).

Generation of single cell clones

Lentivirally transduced and puromycin (InvivoGen, Germany) selected cell lines with the DOX-conditional *AHR* knockdown (bulk level) were seeded in 1:5 collagen coated 96-well plates. To ensure one clone per well, 0.8 cells/well were seeded in a total volume of 200 μL. Medium

contained 40% of pre-filtered (0.45 μm) conditional growth medium of the respective cell lines, supplemented with 20% FCS and 1% penicillin/streptomycin. Growth of the single clones was monitored for 1–2 months and Accutase (Sigma-Aldrich, Germany) was used to transfer them consecutively larger plates and flasks for expansion and further knockdown efficiency testing by qRT-PCR. All single clones were treated with 1 μg/mL DOX (Sigma-Aldrich, Germany) for 96 h, with DOX refreshed every 48 h.

Proliferation assays

For 2D proliferation assays, the trypan blue (Sigma-Aldrich, Germany) exclusion method was used. Cells were seeded at 250,000–400,000 cells/well for MHH-ES-1/TR/shAHR and 300,000–500,000 cells/well for TC-106/TR/shAHR in 6-well plates, then exposed to 1 μg/mL DOX for 96 h (DOX refreshed every 48 h) at which point the cell culture supernatant and cells were collected. For counting cells, 10 µL of cell suspension were mixed 1:1 with trypan blue and live and dead cells counted in four quadrants of a hemocytometer. The proliferation relative to control was determined by calculating the average of all DOX– biological independent controls and dividing all cell numbers of all conditions and biological replicates by that average.

CellTiter-Glo for 3D cell viability assays

For 3D cell viability assays, cells were seeded (MHH-ES-1/TR/shAHR255 and MHH-ES-1/TR/shAHR286: 1,500/well; TC-106/TR/shAHR255 and TC-106/TR/shAHR286: 1,000 cells per well) in 96-well U-bottom low attachment plates (Grenier Bio-one, Germany) to generate a single sphere per well. Spheres were treated with 1 μg/mL DOX for 96 h and DOX was refreshed every 48 h. To determine the effect of AHR silencing on 3D cell viability, a CellTiter-Glo® Cell Viability Luminescent assay (Promega, USA) was performed. After seeding the cells and treating them with DOX for 96 h, spheroids and media blanks (50 µL) were transferred to a white opaque 96-well plate and 50 μL of CellTiter-Glo reagent added per sample. The plate was placed on the shaker for 20 min and luminescence was measured in the GloMax plate reader (1 s integration time). Relative viability compared to the control was calculated.

Colony formation assay

EwS cell lines were seeded at 2,000 cells/well for MHH-ES-1/TR/shAHR or /shControl, and at 1,000 cells/well for TC-106/TR/shAHR or /shControl. After 24 h of seeding, 1 μg/mL of DOX was added and refreshed every 48 h. In addition, 200 μL of only medium were added to both conditions to take into consideration medium evaporation. Crystal violet (Sigma-Aldrich, Germany) staining was performed after 10–12 days. The size and percentage of area of colonies per condition were calculated with the Fiji software (NHI, USA). Relative clonogenicity was calculated normalizing to the controls.

Flow cytometric cell cycle analysis

Propidium iodide (PI) (Bio-Legend, USA) staining was performed for cell cycle analysis. MHH-ES-1/TR/shAHR255 #4 (400,000 cells/well) and TC-106/TR/shAHR286 #23 (500,000 cells/well) were seeded in 6-well plates and 1 μg/mL DOX was added for 96 h. On the day of harvesting, medium was removed from the cells and were washed with ice-cold PBS (ThermoFisher Scientific, USA). Cells were trypsinzed and centrifuged down. After pellet collection cells were washed again with PBS and then fixated with 1 mL of cold 70% ethanol (dropwise). To perform the staining, samples were incubated in the following master mix: 470 μL of flow cytometry staining buffer, 20 μL of PI solution and 10 μL of RNAase (ThermoFisher Scientific, USA). Incubation was performed for 1 h in the dark. Samples acquisition was performed on a BD FACSCanto flow cytometer (BD Biosciences, USA) with 50,000−100,000 events at medium flow rate per sample. Data analysis was performed using the FlowJo v.10.10 software (BD Biosciences, USA), with the percentage of cells present in different cell cycles (sub G1/G0, G1/G0, S and G2/M) determined using the Watson model.

Mouse experiments

All mouse experiments were conducted with the approval of the government of North Baden as the responsible legal authority. The study adhered to the ARRIVE guidelines, European Community and GV-SOLAS recommendations (86/609/EEC), and United Kingdom Coordinating

Committee on Cancer Research (UKCCCR) guidelines for the welfare and use of animals in cancer research. Animals were housed at the central DKFZ animal facility under Specific Opportunist Pathogen-Free (SOPF). Animals had *ad libitum* access to food and water and were housed in individually ventilated cages. Daily assessments of animal well-being were carried out by certified animal caretakers. Mice subcutaneous (s.c.) xenografts and orthotopic xenografts for metastasis assessment were performed as previously described (Cidre-Aranaz and Ohmura, 2021; Cidre-Aranaz *et al.*, 2022). In brief, for s.c. experiments, 3,000,000 EwS cells (MHH-ES-1/TR/shAHR255 #4 or TC-106/TR/shAHR286 #23) resuspended in 100 μL of a 1:1 mix of Geltrex:PBS (ThermoFisher Scientific, USA) were inoculated subcutaneously into the right flank of each NSG mouse. For orthotopic experiments, 200,000 MHH-ES-1/TR/shAHR255 #4 cells were resuspended in 10 μL HBSS 1× and inoculated into the right tibial plateau of each NSG mouse. Once tumors were palpable (s.c.) or the day after injection (orthotopic), mice were randomized and received treatment in the drinking water according to their grouping: control (1.75% sucrose; Sigma-Aldrich, Germany) (DOX−) or treatment (2 mg/mL DOX in 5% sucrose, DOX+). Drinking water was refreshed every 48 h. Primary tumor at the s.c. or orthotopic location were measured every second day with a caliper and volumes were calculated using the following formula: $V = L \times W^2 / 2$, where V is the tumor volume, L the largest diameter and W the smallest diameter. For both s.c. and orthotopic experiments, mice were sacrificed by cervical dislocation at the experimental endpoint or earlier if humane endpoints were reached (body weight loss of 20%, apathy, piloerection, self-isolation, aggression as a sign of pain, self-mutilation, motor abnormalities, as well as any other unphysiological or abnormal body posture, breathing difficulties, maximum tumor size of 15 mm in any direction, an ulcerating tumor or exhibited signs of limping at the injected leg).

DNA isolation

DNA concentration and purity were determined using a NanoDrop One/One UV-Vis spectrophotometer (ThermoFisher Scientific, USA). Genomic DNA for SNP or STR profiling was extracted from fresh or frozen culture cells (10,000−10,000,000 cells) using the NucleoSpin®

Tissue kit as per manufacturer's protocol. Samples for profiling were submitted with a final concentration of 15 ng/μL in 100 μL. DNA from transformed bacteria was isolated using ZymoPURE II Plasmid prep kits as per manufacturer's protocols (Zymo Research, USA). To maximize the amount of DNA isolated, the elution buffer was pre-heated at 70 ºC and added right before the elution to the column. To isolate DNA from the agarose gel, NucleoSpin Gel™ and PCR Clean-up kits (Macherey-Nagel, Germany) were used according to the manufacturer's protocol.

Immunoblotting

AHR silencing was confirmed at the protein level. All single clones were treated with 1 μg/mL DOX for 96 h and DOX was refreshed every 48 h. Cells were collected following 96 h DOX treatment and lysed in RIPA buffer containing phosphatase inhibitor and protease inhibitor. Protein was quantified by Pierce BCA Protein Assay Kit (ThermoFisher Scientific, USA) as per manufacture's protocol. Samples (20 μg whole cell lysate with 6× Laemmli loading buffer in a total volume of 20 μL) were run on 10% Tris-HCl gels (Bio-Rad, Hercules, CA, USA). Meanwhile, PVDF membrane was activated in 100% methanol the equilibrated in transfer buffer. Proteins were transferred to the membrane at 1.0A for 7 min using the Turbo transfer system (Bio-Rad). Membrane was rinsed in TBS-T then blocked in 5% milk/TBS-T for 1 h at room temperature. Membranes were washed three times for 5 min in TBS-T then incubated with 1:1,000 anti-AHR (D5S6H clone, #83200, Cell Signaling Technologies, Danvers, MA, USA) or 1:1,000 anti-GAPDH (14C10 clone, #2118S, Cell Signaling Technologies) antibodies in 5% milk/TBS-T, overnight at 4 ºC. Membranes were then washed three times for 5 min with TBS-T and then incubated with HRP-conjugated goat anti-rabbit secondary (1:2,000, 5% milk/TBS-T, 2 h, room temperature; #31460, ThermoFisher Scientific). Then, the membrane was washed three times for 5 min in TBS-T and incubated with WesternBright chemiluminescence substrate (Biozym, Germany) for 2 min. Proteins were visualized using the FusionFX Western Blot & Chemi imaging system (Vilber, France).

Drug-response assays

MHH-ES-1 and TC-106 cells were seeded (4,000 cells/well) in 96-well plates and treated with the AHR inhibitor GNF-351 (MedChemExpress, USA; 200 mM in DMSO) for 72 h. Resazurin assay was performed to determined cell viability as described above. CFA assays were performed in a dose-dependent matter by treating EwS cells with GNF-351 for 72 h. Staining of colonies and analysis was performed as described before.

Statistics

Statistical analysis of both *in vitro* and *in vivo* experiments was performed using GraphPad PRISM 10.1.2 (GraphPad Software, USA). Data were presented as mean ± standard error of the mean (SEM), and one- or two-tailed Mann-Whitney test was performed.

REFERENCES

Aggen, D.H. *et al.* (2024) 'IK-175, an oral AHR inhibitor, as monotherapy and in combination with nivolumab in patients with urothelial carcinoma resistant/refractory to PD-1/L1 inhibitors.', *Journal of Clinical Oncology*, 42(16_suppl), pp. 2599–2599. Available at: https://doi.org/10.1200/JCO.2024.42.16_suppl.2599.

Altvater, B. *et al.* (2021) 'HLA-G and HLA-E Immune Checkpoints Are Widely Expressed in Ewing Sarcoma but Have Limited Functional Impact on the Effector Functions of Antigen-Specific CAR T Cells', *Cancers*, 13(12). Available at: https://doi.org/10.3390/cancers13122857.

Arase, H., Arase, N. and Saito, T. (1996) 'Interferon gamma production by natural killer (NK) cells and NK1.1+ T cells upon NKR-P1 cross-linking.', *Journal of Experimental Medicine*, 183(5), pp. 2391–2396. Available at: https://doi.org/10.1084/jem.183.5.2391.

Aynaud, M.-M. *et al.* (2020) 'Transcriptional Programs Define Intratumoral Heterogeneity of Ewing Sarcoma at Single-Cell Resolution', *Cell Reports*, 30(6), pp. 1767-1779.e6. Available at: https://doi.org/10.1016/j.celrep.2020.01.049.

Barbie, D.A. *et al.* (2009) 'Systematic RNA interference reveals that oncogenic KRAS-driven cancers require TBK1', *Nature*, 462(7269), pp. 108–112. Available at: https://doi.org/10.1038/nature08460.

Cantor, J.R. *et al.* (2017) 'Physiologic Medium Rewires Cellular Metabolism and Reveals Uric Acid as an Endogenous Inhibitor of UMP Synthase', *Cell*, 169(2), pp. 258-272.e17. Available at: https://doi.org/10.1016/j.cell.2017.03.023.

Ceranski, A.K. *et al.* (2025) 'Refined culture conditions with increased physiological relevance uncover oncogene-dependent metabolic signatures in Ewing sarcoma spheroids', *Cell Reports Methods*, p. 100966. Available at: https://doi.org/10.1016/j.crmeth.2025.100966.

Charoentong, P. *et al.* (2017) 'Pan-cancer Immunogenomic Analyses Reveal Genotype-Immunophenotype Relationships and Predictors of Response to Checkpoint Blockade', *Cell Reports*, 18(1), pp. 248–262. Available at: https://doi.org/10.1016/j.celrep.2016.12.019.

Chaturvedi, A. *et al.* (2012) 'The EWS/FLI Oncogene Drives Changes in Cellular Morphology, Adhesion, and Migration in Ewing Sarcoma', *Genes & Cancer*, 3(2), pp. 102–116. Available at: https://doi.org/10.1177/1947601912457024.

Chaturvedi, A. *et al.* (2014) 'Molecular dissection of the mechanism by which EWS/FLI expression compromises actin cytoskeletal integrity and cell adhesion in Ewing sarcoma', *Molecular Biology of the Cell*. Edited by P. Forscher, 25(18), pp. 2695–2709. Available at: https://doi.org/10.1091/mbc.e14-01-0007.

Chiesa, M.D. *et al.* (2006) 'The tryptophan catabolite l-kynurenine inhibits the surface expression of NKp46- and NKG2D-activating receptors and regulates NK-cell function', *Blood*, 108(13), pp. 4118–4125. Available at: https://doi.org/10.1182/blood-2006-03-006700.

Cidre-Aranaz, F. *et al.* (2022) 'Integrative gene network and functional analyses identify a prognostically relevant key regulator of metastasis in Ewing sarcoma', *Molecular Cancer*, 21(1), p. 1. Available at: https://doi.org/10.1186/s12943-021-01470-z.

Cidre-Aranaz, F. and Ohmura, S. (2021) 'Tumor Growth Analysis of Ewing Sarcoma Cell Lines Using Subcutaneous Xenografts in Mice', in F. Cidre-Aranaz and T. G. P. Grünewald (eds) *Ewing Sarcoma : Methods and Protocols*. New York, NY: Springer US, pp. 191–199. Available at: https://doi.org/10.1007/978-1-0716-1020-6_15.

D'Amato, N.C. *et al.* (2015) 'A TDO2-AhR Signaling Axis Facilitates Anoikis Resistance and Metastasis in Triple-Negative Breast Cancer', *Cancer Research*, 75(21), pp. 4651–4664. Available at: https://doi.org/10.1158/0008-5472.CAN-15-2011.

Davis, K.L. *et al.* (2020) 'Nivolumab in children and young adults with relapsed or refractory solid tumours or lymphoma (ADVL1412): a multicentre, open-label, single-arm, phase 1–2 trial', *The Lancet Oncology*, 21(4), pp. 541–550. Available at: https://doi.org/10.1016/S1470-2045(20)30023-1.

Delattre *et al.* (1994) 'The Ewing Family of Tumors -- A Subgroup of Small-Round-Cell Tumors Defined by Specific Chimeric Transcripts', *New England Journal of Medicine*, 331(5), pp. 294–299. Available at: https://doi.org/10.1056/NEJM199408043310503.

Delattre, O. *et al.* (1992) 'Gene fusion with an ETS DNA-binding domain caused by chromosome translocation in human tumours', *Nature*, 359(6391), pp. 162–165. Available at: https://doi.org/10.1038/359162a0.

Dietrich, C. and Kaina, B. (2010) 'The aryl hydrocarbon receptor (AhR) in the regulation of cell-cell contact and tumor growth', *Carcinogenesis*, 31(8), pp. 1319–1328. Available at: https://doi.org/10.1093/carcin/bgq028.

DiNatale, B.C. *et al.* (2010) 'Kynurenic Acid Is a Potent Endogenous Aryl Hydrocarbon Receptor Ligand that Synergistically Induces Interleukin-6 in the Presence of Inflammatory Signaling', *Toxicological Sciences*, 115(1), pp. 89–97. Available at: https://doi.org/10.1093/toxsci/kfq024.

Evans, J.D. (1996) *Straightforward statistics for the behavioral sciences*. Pacific Grove: Brooks/Cole Pub. Co.

Evdokimova, V. *et al.* (2023) 'Current State of Immunotherapy and Mechanisms of Immune Evasion in Ewing Sarcoma and Osteosarcoma', *Cancers*, 15(1). Available at: https://doi.org/10.3390/cancers15010272.

Franzetti, G.-A. *et al.* (2017) 'Cell-to-cell heterogeneity of EWSR1-FLI1 activity determines proliferation/migration choices in Ewing sarcoma cells', *Oncogene*, 36(25), pp. 3505–3514. Available at: https://doi.org/10.1038/onc.2016.498.

Fujiwara, T. *et al.* (2011) 'Macrophage Infiltration Predicts a Poor Prognosis for Human Ewing Sarcoma', *The American Journal of Pathology*, 179(3), pp. 1157–1170. Available at: https://doi.org/10.1016/j.ajpath.2011.05.034.

Gautier, L. *et al.* (2004) 'affy—analysis of Affymetrix GeneChip data at the probe level', *Bioinformatics*, 20(3), pp. 307–315. Available at: https://doi.org/10.1093/bioinformatics/btg405.

Greene, L.I. *et al.* (2019) 'A Role for Tryptophan-2,3-dioxygenase in CD8 T-cell Suppression and Evidence of Tryptophan Catabolism in Breast Cancer Patient Plasma', *Molecular Cancer Research*, 17(1), pp. 131–139. Available at: https://doi.org/10.1158/1541-7786.MCR-18-0362.

Grünewald, T.G. *et al.* (2020) 'Sarcoma treatment in the era of molecular medicine', *EMBO Molecular Medicine*, 12(11). Available at: https://doi.org/10.15252/emmm.201911131.

Grünewald, T.G.P. *et al.* (2018) 'Ewing sarcoma', *Nature Reviews Disease Primers*, 4(1), p. 5. Available at: https://doi.org/10.1038/s41572-018-0003-x.

van Gulijk, M. *et al.* (2023) 'PD-L1 checkpoint blockade promotes regulatory T cell activity that underlies therapy resistance', *Science Immunology*, 8(83), p. eabn6173. Available at: https://doi.org/10.1126/sciimmunol.abn6173.

Gutiérrez-Vázquez, C. and Quintana, F.J. (2018) 'Regulation of the Immune Response by the Aryl Hydrocarbon Receptor', *Immunity*, 48(1), pp. 19–33. Available at: https://doi.org/10.1016/j.immuni.2017.12.012.

Hänzelmann, S., Castelo, R. and Guinney, J. (2013) 'GSVA: gene set variation analysis for microarray and RNA-Seq data', *BMC Bioinformatics*, 14(1), p. 7. Available at: https://doi.org/10.1186/1471-2105-14-7.

Hess, D. *et al.* (2025) 'Abstract CT074: Discovery and preliminary clinical findings of MK-6598, a potent and selective inhibitor of the immune checkpoint IL4I1', *Cancer Research*, 85(8_Supplement_2), pp. CT074–CT074. Available at: https://doi.org/10.1158/1538-7445.AM2025-CT074.

Holfelder, P. *et al.* (2024) 'The MTORC1-AHR pathway sustains translation and autophagy in tumours under tryptophan stress', *bioRxiv*, p. 2023.01.16.523931. Available at: https://doi.org/10.1101/2023.01.16.523931.

Hou, A. *et al.* (2020) 'Targeting Myeloid-Derived Suppressor Cell, a Promising Strategy to Overcome Resistance to Immune Checkpoint Inhibitors', *Frontiers in Immunology*, 11, p. 783. Available at: https://doi.org/10.3389/fimmu.2020.00783.

Irizarry, R.A. *et al.* (2003) 'Exploration, normalization, and summaries of high density oligonucleotide array probe level data', *Biostatistics*, 4(2), pp. 249–264. Available at: https://doi.org/10.1093/biostatistics/4.2.249.

Issaq, S.H. *et al.* (2020) 'EWS-FLI1–regulated Serine Synthesis and Exogenous Serine are Necessary for Ewing Sarcoma Cellular Proliferation and Tumor Growth', *Molecular Cancer Therapeutics*, 19(7), pp. 1520–1529. Available at: https://doi.org/10.1158/1535-7163.MCT-19-0748.

Jung, K.H. *et al.* (2019) 'Phase I Study of the Indoleamine 2,3-Dioxygenase 1 (IDO1) Inhibitor Navoximod (GDC-0919) Administered with PD-L1 Inhibitor (Atezolizumab) in Advanced Solid Tumors', *Clinical Cancer Research*, 25(11), pp. 3220–3228. Available at: https://doi.org/10.1158/1078-0432.CCR-18-2740.

Kaur, K., Celis, A.P. and Jewett, A. (2025) 'Natural Killer Cell-Secreted IFN-γ and TNF-α Mediated Differentiation in Lung Stem-like Tumors, Leading to the Susceptibility of the Tumors to Chemotherapeutic Drugs', *Cells*, 14(2). Available at: https://doi.org/10.3390/cells14020090.

Klingemann, H. (2023) 'The NK-92 cell line—30 years later: its impact on natural killer cell research and treatment of cancer', *Cytotherapy*, 25(5), pp. 451–457. Available at: https://doi.org/10.1016/j.jcyt.2022.12.003.

Kober, C. *et al.* (2023) 'Targeting the aryl hydrocarbon receptor (AhR) with BAY 2416964: a selective small molecule inhibitor for cancer immunotherapy', *Journal for ImmunoTherapy of Cancer*, 11(11), p. e007495. Available at: https://doi.org/10.1136/jitc-2023-007495.

Kozlova, A. and and Frédérick, R. (2019) 'Current state on tryptophan 2,3-dioxygenase inhibitors: a patent review', *Expert Opinion on Therapeutic Patents*, 29(1), pp. 11–23. Available at: https://doi.org/10.1080/13543776.2019.1556638.

Langfelder, P. and Horvath, S. (2008) 'WGCNA: an R package for weighted correlation network analysis', *BMC Bioinformatics*, 9(1), p. 559. Available at: https://doi.org/10.1186/1471-2105-9-559.

Lewis, H.C. *et al.* (2017) 'The IDO inhibitor 1-methyl tryptophan activates the aryl hydrocarbon receptor response in mesenchymal stromal cells', *Oncotarget*, 8(54), pp. 91914–91927. Available at: https://doi.org/10.18632/oncotarget.20166.

Liu, X.-D. *et al.* (2015) 'Resistance to Antiangiogenic Therapy Is Associated with an Immunosuppressive Tumor Microenvironment in Metastatic Renal Cell Carcinoma', *Cancer Immunology Research*, 3(9), pp. 1017–1029. Available at: https://doi.org/10.1158/2326-6066.CIR-14-0244.

Liu, Y. *et al.* (2018) 'Tumor-Repopulating Cells Induce PD-1 Expression in CD8+ T Cells by Transferring Kynurenine and AhR Activation', *Cancer Cell*, 33(3), pp. 480-494.e7. Available at: https://doi.org/10.1016/j.ccell.2018.02.005.

Livak, K.J. and Schmittgen, T.D. (2001) 'Analysis of Relative Gene Expression Data Using Real-Time Quantitative PCR and the 2−ΔΔCT Method', *Methods*, 25(4), pp. 402–408. Available at: https://doi.org/10.1006/meth.2001.1262.

Long, G.V. *et al.* (2019) 'Epacadostat plus pembrolizumab versus placebo plus pembrolizumab in patients with unresectable or metastatic melanoma (ECHO-301/KEYNOTE-252): a phase 3, randomised, double-blind study', *The Lancet Oncology*, 20(8), pp. 1083–1097. Available at: https://doi.org/10.1016/S1470-2045(19)30274-8.

Luo, W. *et al.* (2024) 'Combinatorial macrophage induced innate immunotherapy against Ewing sarcoma: Turning "Two Keys" simultaneously', *Journal of Experimental & Clinical Cancer Research*, 43(1), p. 193. Available at: https://doi.org/10.1186/s13046-024-03093-w.

MacKinnon, A. *et al.* (2020) '705 Anti-tumor activity of CB-668, a potent, selective and orally bioavailable small-molecule inhibitor of the immuno-suppressive enzyme Interleukin 4 (IL-4)-Induced Gene 1 (IL4I1)', *Journal for ImmunoTherapy of Cancer*, 8(Suppl 3), p. A423. Available at: https://doi.org/10.1136/jitc-2020-SITC2020.0705.

Malempati, S. *et al.* (2012) 'Phase I/II Trial and Pharmacokinetic Study of Cixutumumab in Pediatric Patients With Refractory Solid Tumors and Ewing Sarcoma: A Report From the Children's Oncology Group', *Journal of Clinical Oncology*, 30(3), pp. 256–262. Available at: https://doi.org/10.1200/JCO.2011.37.4355.

May, W.A. *et al.* (1993) 'Ewing sarcoma 11;22 translocation produces a chimeric transcription factor that requires the DNA-binding domain encoded by FLI1 for transformation.', *Proceedings of the National Academy of Sciences*, 90(12), pp. 5752–5756. Available at: https://doi.org/10.1073/pnas.90.12.5752.

Mayoh, C. *et al.* (2023) 'A novel transcriptional signature identifies T-cell infiltration in high-risk paediatric cancer', *Genome Medicine*, 15(1), p. 20. Available at: https://doi.org/10.1186/s13073-023-01170-x.

Mezrich, J.D. *et al.* (2010) 'An Interaction between Kynurenine and the Aryl Hydrocarbon Receptor Can Generate Regulatory T Cells', *The Journal of Immunology*, 185(6), pp. 3190–3198. Available at: https://doi.org/10.4049/jimmunol.0903670.

Moyer, B.J. *et al.* (2017) 'Indoleamine 2,3-dioxygenase 1 (IDO1) inhibitors activate the aryl hydrocarbon receptor', *Toxicology and Applied Pharmacology*, 323, pp. 74–80. Available at: https://doi.org/10.1016/j.taap.2017.03.012.

Murray, I.A., Patterson, A.D. and Perdew, G.H. (2014) 'Aryl hydrocarbon receptor ligands in cancer: friend and foe', *Nature Reviews Cancer*, 14(12), pp. 801–814. Available at: https://doi.org/10.1038/nrc3846.

Musa, J. *et al.* (2019) 'Cooperation of cancer drivers with regulatory germline variants shapes clinical outcomes', *Nature Communications*, 10(1), p. 4128. Available at: https://doi.org/10.1038/s41467-019-12071-2.

Musa, J. (2021) *Integrative characterization of the cooperation between EWSR1-FLI1 and regulatory germline variants in tumor progression of Ewing sarcoma*. Medical Dissertation. Faculty of Medicine, Ludwig-Maximilians University of Munich.

Musa, J. and Cidre-Aranaz, F. (2021) 'Drug Screening by Resazurin Colorimetry in Ewing Sarcoma', in F. Cidre-Aranaz and T. G. P. Grünewald (eds) *Ewing Sarcoma : Methods and Protocols*. New York, NY: Springer US, pp. 159–166. Available at: https://doi.org/10.1007/978-1-0716-1020-6_12.

Mutz, C.N. *et al.* (2016) 'EWS-FLI1 impairs aryl hydrocarbon receptor activation by blocking tryptophan breakdown via the kynurenine pathway', *FEBS Letters*, 590(14), pp. 2063–2075. Available at: https://doi.org/10.1002/1873-3468.12243.

Neamah, W.H., Nagarkatti, P. and Nagarkatti, M. (2018) '2,3,7,8 tetrachlorodibenzo-p-dioxin (TCDD)-induced myeloid derived suppressor cells (MDSC) have heightened metabolic activity which correlates with microRNA and gene expression involved in immunosuppression', *The Journal of Immunology*, 200(1_Supplement), p. 46.1-46.1. Available at: https://doi.org/10.4049/jimmunol.200.Supp.46.1.

Novikov, O. *et al.* (2016) 'An Aryl Hydrocarbon Receptor-Mediated Amplification Loop That Enforces Cell Migration in ER−/PR−/Her2− Human Breast Cancer Cells', *Molecular Pharmacology*, 90(5), pp. 674–688. Available at: https://doi.org/10.1124/mol.116.105361.

Opitz, C.A. *et al.* (2011) 'An endogenous tumour-promoting ligand of the human aryl hydrocarbon receptor', *Nature*, 478(7368), pp. 197–203. Available at: https://doi.org/10.1038/nature10491.

Opitz, C.A. *et al.* (2020) 'The therapeutic potential of targeting tryptophan catabolism in cancer', *British Journal of Cancer*, 122(1), pp. 30–44. Available at: https://doi.org/10.1038/s41416-019-0664-6.

Opitz, C.A. *et al.* (2023) 'The complex biology of aryl hydrocarbon receptor activation in cancer and beyond', *Biochemical Pharmacology*, 216, p. 115798. Available at: https://doi.org/10.1016/j.bcp.2023.115798.

Orth, M.F. *et al.* (2022) 'Systematic multi-omics cell line profiling uncovers principles of Ewing sarcoma fusion oncogene-mediated gene regulation', *Cell Reports*, 41(10), p. 111761. Available at: https://doi.org/10.1016/j.celrep.2022.111761.

Oweida, A. *et al.* (2018) 'Resistance to Radiotherapy and PD-L1 Blockade Is Mediated by TIM-3 Upregulation and Regulatory T-Cell Infiltration', *Clinical Cancer Research*, 24(21), pp. 5368–5380. Available at: https://doi.org/10.1158/1078-0432.CCR-18-1038.

Pelossof, R. *et al.* (2017) 'Prediction of potent shRNAs with a sequential classification algorithm', *Nature Biotechnology*, 35(4), pp. 350–353. Available at: https://doi.org/10.1038/nbt.3807.

Peng, T.-L. *et al.* (2009) 'Aryl hydrocarbon receptor pathway activation enhances gastric cancer cell invasiveness likely through a c-Jun-dependent induction of matrix metalloproteinase-9', *BMC Cell Biology*, 10(1), p. 27. Available at: https://doi.org/10.1186/1471-2121-10-27.

Petrova, V. *et al.* (2023) 'Immunosuppressive capacity of circulating MDSC predicts response to immune checkpoint inhibitors in melanoma patients', *Frontiers in Immunology*, 14, p. 1065767. Available at: https://doi.org/10.3389/fimmu.2023.1065767.

Platten, M. *et al.* (2019) 'Tryptophan metabolism as a common therapeutic target in cancer, neurodegeneration and beyond', *Nature Reviews Drug Discovery*, 18(5), pp. 379–401. Available at: https://doi.org/10.1038/s41573-019-0016-5.

Postel-Vinay, S. *et al.* (2012) 'Common variants near TARDBP and EGR2 are associated with susceptibility to Ewing sarcoma', *Nature Genetics*, 44(3), pp. 323–327. Available at: https://doi.org/10.1038/ng.1085.

Puga, A., Xia, Y. and Elferink, C. (2002) 'Role of the aryl hydrocarbon receptor in cell cycle regulation', *Chemico-Biological Interactions*, 141(1), pp. 117–130. Available at: https://doi.org/10.1016/S0009-2797(02)00069-8.

Quintana, F.J. *et al.* (2008) 'Control of Treg and TH17 cell differentiation by the aryl hydrocarbon receptor', *Nature*, 453(7191), pp. 65–71. Available at: https://doi.org/10.1038/nature06880.

Ritchie, M.E. *et al.* (2015) 'limma powers differential expression analyses for RNA-sequencing and microarray studies', *Nucleic Acids Research*, 43(7), pp. e47–e47. Available at: https://doi.org/10.1093/nar/gkv007.

Rothhammer, V. and Quintana, F.J. (2019) 'The aryl hydrocarbon receptor: an environmental sensor integrating immune responses in health and disease', *Nature Reviews Immunology*, 19(3), pp. 184–197. Available at: https://doi.org/10.1038/s41577-019-0125-8.

Sadik, A. *et al.* (2020) 'IL4I1 Is a Metabolic Immune Checkpoint that Activates the AHR and Promotes Tumor Progression', *Cell*, 182(5), pp. 1252-1270.e34. Available at: https://doi.org/10.1016/j.cell.2020.07.038.

Sannino, G. *et al.* (2017) 'Epithelial-to-Mesenchymal and Mesenchymal-to-Epithelial Transition in Mesenchymal Tumors: A Paradox in Sarcomas?', *Cancer Research*, 77(17), pp. 4556–4561. Available at: https://doi.org/10.1158/0008-5472.CAN-17-0032.

Savola, S. *et al.* (2011) 'High Expression of Complement Component 5 (C5) at Tumor Site Associates with Superior Survival in Ewing′s Sarcoma Family of Tumour Patients', *International Scholarly Research Notices*, 2011(1), p. 168712. Available at: https://doi.org/10.5402/2011/168712.

Scotlandi, K. *et al.* (2009) 'Overcoming Resistance to Conventional Drugs in Ewing Sarcoma and Identification of Molecular Predictors of Outcome', *Journal of Clinical Oncology*, 27(13), pp. 2209–2216. Available at: https://doi.org/10.1200/JCO.2008.19.2542.

Sen, N. *et al.* (2018) 'EWS-FLI1 reprograms the metabolism of Ewing sarcoma cells via positive regulation of glutamine import and serine-glycine biosynthesis', *Molecular Carcinogenesis*, 57(10), pp. 1342–1357. Available at: https://doi.org/10.1002/mc.22849.

Shadboorestan, A. *et al.* (2019) 'Invasion and migration of MDA-MB-231 cells are inhibited by block of AhR and NFAT: role of AhR/NFAT1/β4 integrin signaling', *Journal of Applied Toxicology*, 39(2), pp. 375–384. Available at: https://doi.org/10.1002/jat.3728.

Smith, K.J. *et al.* (2011) 'Identification of a High-Affinity Ligand That Exhibits Complete Aryl Hydrocarbon Receptor Antagonism', *The Journal of Pharmacology and Experimental Therapeutics*, 338(1), pp. 318–327. Available at: https://doi.org/10.1124/jpet.110.178392.

Solvay, M. *et al.* (2023) 'Tryptophan depletion sensitizes the AHR pathway by increasing AHR expression and GCN2/LAT1-mediated kynurenine uptake, and potentiates induction of regulatory T lymphocytes', *Journal for ImmunoTherapy of Cancer*, 11(6), p. e006728. Available at: https://doi.org/10.1136/jitc-2023-006728.

Sorensen, P.H.B. *et al.* (1994) 'A second Ewing's sarcoma translocation, t(21;22), fuses the EWS gene to another ETS–family transcription factor, ERG', *Nature Genetics*, 6(2), pp. 146–151. Available at: https://doi.org/10.1038/ng0294-146.

Spurny, C. *et al.* (2017) 'T cell infiltration into Ewing sarcomas is associated with local expression of immune-inhibitory HLA-G', *Oncotarget; Vol 9, No 5* [Preprint]. Available at: https://www.oncotarget.com/article/23815/text/ (Accessed: 1 January 2017).

Stahl, M. *et al.* (2011) 'Risk of recurrence and survival after relapse in patients with Ewing sarcoma', *Pediatric Blood & Cancer*, 57(4), pp. 549–553. Available at: https://doi.org/10.1002/pbc.23040.

Stanford, E.A. *et al.* (2016) 'Role for the Aryl Hydrocarbon Receptor and Diverse Ligands in Oral Squamous Cell Carcinoma Migration and Tumorigenesis', *Molecular Cancer Research*, 14(8), pp. 696–706. Available at: https://doi.org/10.1158/1541-7786.MCR-16-0069.

Tawbi, H.A. *et al.* (2017) 'Pembrolizumab in advanced soft-tissue sarcoma and bone sarcoma (SARC028): a multicentre, two-cohort, single-arm, open-label, phase 2 trial', *The Lancet Oncology*, 18(11), pp. 1493–1501. Available at: https://doi.org/10.1016/S1470-2045(17)30624-1.

Therneau, T.M. (2024) 'survival: Survival Analysis'. Available at: https://doi.org/10.32614/CRAN.package.survival.

Therneau, T.M. and Grambsch, P.M. (2000) *Modeling Survival Data: Extending the Cox Model*. New York, NY: Springer New York (Statistics for Biology and Health). Available at: https://doi.org/10.1007/978-1-4757-3294-8.

Tomazou, E.M. *et al.* (2015) 'Epigenome Mapping Reveals Distinct Modes of Gene Regulation and Widespread Enhancer Reprogramming by the Oncogenic Fusion Protein EWS-FLI1', *Cell Reports*, 10(7), pp. 1082–1095. Available at: https://doi.org/10.1016/j.celrep.2015.01.042.

Trikha, P. *et al.* (2021) 'Defining the AHR-regulated transcriptome in NK cells reveals gene expression programs relevant to development and function', *Blood Advances*, 5(22), pp. 4605–4618. Available at: https://doi.org/10.1182/bloodadvances.2021004533.

Van Den Bogaard, E.H. *et al.* (2015) 'Genetic and Pharmacological Analysis Identifies a Physiological Role for the AHR in Epidermal Differentiation', *Journal of Investigative Dermatology*, 135(5), pp. 1320–1328. Available at: https://doi.org/10.1038/jid.2015.6.

Vande Voorde, J. *et al.* (2019) 'Improving the metabolic fidelity of cancer models with a physiological cell culture medium', *Science Advances*, 5(1), p. eaau7314. Available at: https://doi.org/10.1126/sciadv.aau7314.

Visser, L.L. *et al.* (2023) 'Ewing Sarcoma Single-cell Transcriptome Analysis Reveals Functionally Impaired Antigen-presenting Cells', *Cancer Research Communications*, 3(10), pp. 2158–2169. Available at: https://doi.org/10.1158/2767-9764.CRC-23-0027.

Volchenboum, S.L. *et al.* (2015) 'Gene expression profiling of Ewing sarcoma tumours reveals the prognostic importance of tumour–stromal interactions: a report from the Children's Oncology Group', *The Journal of Pathology: Clinical Research*, 1(2), pp. 83–94. Available at: https://doi.org/10.1002/cjp2.9.

Weber, R. *et al.* (2018) 'Myeloid-Derived Suppressor Cells Hinder the Anti-Cancer Activity of Immune Checkpoint Inhibitors', *Frontiers in Immunology*, 9, p. 1310. Available at: https://doi.org/10.3389/fimmu.2018.01310.

Wiles, E.T. *et al.* (2013) 'ZEB2 Represses the Epithelial Phenotype and Facilitates Metastasis in Ewing Sarcoma', *Genes & Cancer*, 4(11–12), pp. 486–500. Available at: https://doi.org/10.1177/1947601913506115.

Wilkerson, M.D. and Hayes, D.N. (2010) 'ConsensusClusterPlus: a class discovery tool with confidence assessments and item tracking', *Bioinformatics*, 26(12), pp. 1572–1573. Available at: https://doi.org/10.1093/bioinformatics/btq170.

Ye, M. *et al.* (2018) 'Activation of the Aryl Hydrocarbon Receptor Leads to Resistance to EGFR TKIs in Non–Small Cell Lung Cancer by Activating Src-mediated Bypass Signaling', *Clinical Cancer Research*, 24(5), pp. 1227–1239. Available at: https://doi.org/10.1158/1078-0432.CCR-17-0396.

Yin, X.-F. *et al.* (2012) 'A selective aryl hydrocarbon receptor modulator 3,3'-Diindolylmethane inhibits gastric cancer cell growth', *Journal of Experimental & Clinical Cancer Research*, 31(1), p. 46. Available at: https://doi.org/10.1186/1756-9966-31-46.

Supplementary Table 1.

Name/Clone ID	Sequence 5' to 3'	Purpose
shRNA_AHR_255_F (TRCN0000021255)	CCGGGCTTCTTTGATGTTGCATTAACTCGAGTTAATGCAACATCAAAGAAGCTTTTTG	Cloning
shRNA_AHR_255_R (TRCN0000021255)	AATTCAAAAAGCTTCTTTGATGTTGCATTAACTCGAGTTAATGCAACATCAAAGAAGC	Cloning
sh_AHR_F_286 (TRCN0000245286)	CCGGATCCACAGTCAGCCATAATAACTCGAGTTATTATGGCTGACTGTGGATTTTTTG	Cloning
sh_AHR_R_286 (TRCN0000245286)	AATTCAAAAAATCCACAGTCAGCCATAATAACTCGAGTTATTATGGCTGACTGTGGAT	Cloning
TETpLKO_colony_F	GGCAGGGATATTCACCATTAT	PCR
TETpLKO_colony_R	CTATTCTTTCCCCTGCACTG	PCR
TETpLKOseqF	GGCAGGGATATTCACCATTATCGTTTCAGA	Sequencing
TETpLKOseqR	GACGTGAAGAATGTGCGAGA	Sequencing
RPLP0_F	GAAACTCTGCATTCTCGCTTC	qRT-PCR
RPLP0_R	GGTGTAATCCGTCTCCACAG	qRT-PCR
EF1_743forEWS_F	GCCAAGCTCCAAGTCAATATAGC	qRT-PCR
EF2_852forFLI1_R	GAGGCCAGAATTCATGTTATTGC	qRT-PCR
EWSR1_ERG_F	TCCAAGTCAATATAGCCAACAGAG	qRT-PCR
EWSR1_ERG_R	CTGTGGAAGGAGATGGTTGAG	qRT-PCR
AHR_F	CCAACATCACCTACGCCAGT	qRT-PCR
AHR_R	CCAAACGGTCCAACTCTGTAT	qRT-PCR
IL4I1_qPCR_F	GCAGAAAGGCGATGAAGAAG	qRT-PCR
IL4I1_qPCR_R	GACATCACGTCTCCCAGAAG	qRT-PCR
TDO2_qPCR_F	CAAATCCTCTGGGAGTTGGA	qRT-PCR
TDO2_qPCR_R	GTCCAAGGCTGTCATCGTCT	qRT-PCR
KMO_qPCR_F	TAGCCCTTTCTCATAGAGGACG	qRT-PCR
KMO_qPCR_R	CTCTCATGGGAATACCTTGGGA	qRT-PCR

FIGURES

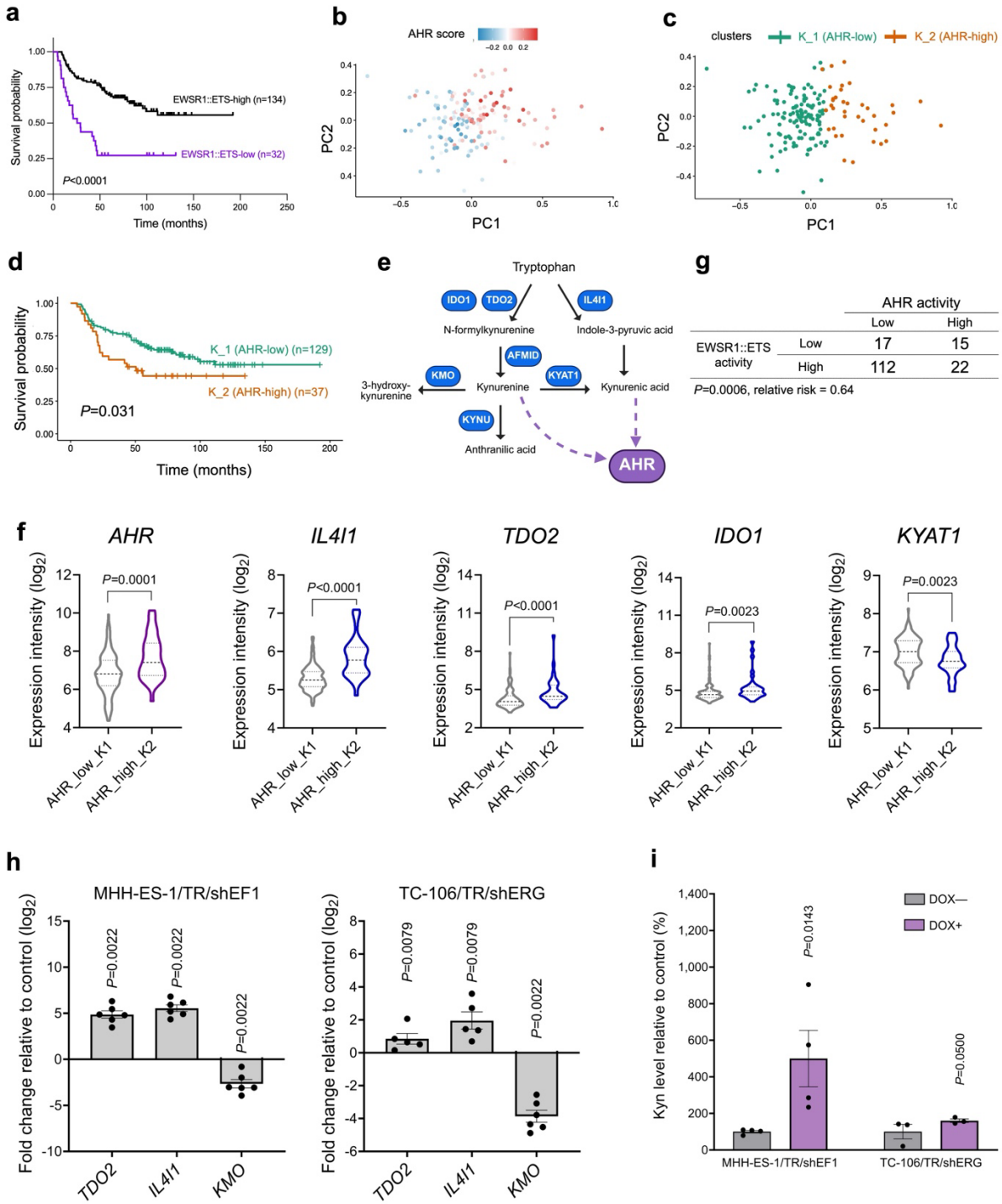

Figure 1. High AHR activity confers worse overall survival in EwS patients and correlates with EWSR1::ETS-low activity.

a) Gene expression microarray data from EwS tumors (n=166) with matched survival data. Kaplan-Meier analysis of patient overall survival was performed on patients divided into EWSR1::ETS-high and -low groups based on ssGSEA scoring and subsequent K-means clustering. **b,c)** K-means clustering of patients within the n=166 cohort identified two clusters: K1 (AHR-signaling low) and K2 (AHR-signaling high) with different AHR activity scores based on a published mRNA signature. **d)** Kaplan-Meier analysis of patient overall survival comparing patients stratified into AHR-signaling low (K1) and high (K2) (log-rank test). **e)** Kynurenine pathway scheme showing the steps and the enzymes involved in tryptophan catabolism. TDO2: tryptophan 2,3-dioxygenase. IL4I1: interleukin-4-induced-1. IDO1: indoleamine 2,3-dioxygenase 1. KYAT1: Kyn aminotransferase 1. KMO: Kyn 3-monooxygenase. KYNU: kynureninase. AHR: aryl hydrocarbon receptor. Created in BioRender. Carreno Gonzalez, M. (2025). https:// BioRender.com/kuuj1i8. **f)** Expression levels of Trp-Kyn pathway enzymes (not present in the AHR signaling signature) *AHR*, *IL4I1*, *TDO2*, *IDO1*, and *KYAT1* in tumors stratified into AHR-low (K1) or -high (K2) in the n=166 EwS cohort. *P*-values were determined by two-tailed Mann-Whitney test. **g)** Contingency table showing distribution of EWSR1::ETS and AHR activity score-based

clusters in EwS tumors (n=166). *P*-value was determined by two tailed Fisher's exact test. **h)** Expression levels of *TDO2*, *IL4I1* and *KMO* upon knockdown of *EWSR1::FLI1* and *EWSR1::ERG* fusions (96 h DOX treatment) in MHH-ES-1/TR/shEF1 and TC-106/TR/shERG. Horizontal bars represent the mean and whiskers the SEM. n=5–6 biologically independent experiments. *P*-values were determined by two-tailed Mann-Whitney test. **i)** Percentage of Kyn levels relative to control upon knockdown of *EWSR1::FLI1* and *EWSR1::ERG* fusions in MHH-ES-1/TR/shEF1 and TC-106/TR/shERG in 3D HPLMax 7% FCS. Horizontal bars represent the mean and whiskers the SEM. n=3–4 biologically independent experiments. *P*-values from were determined by one-tailed Mann-Whitney test.

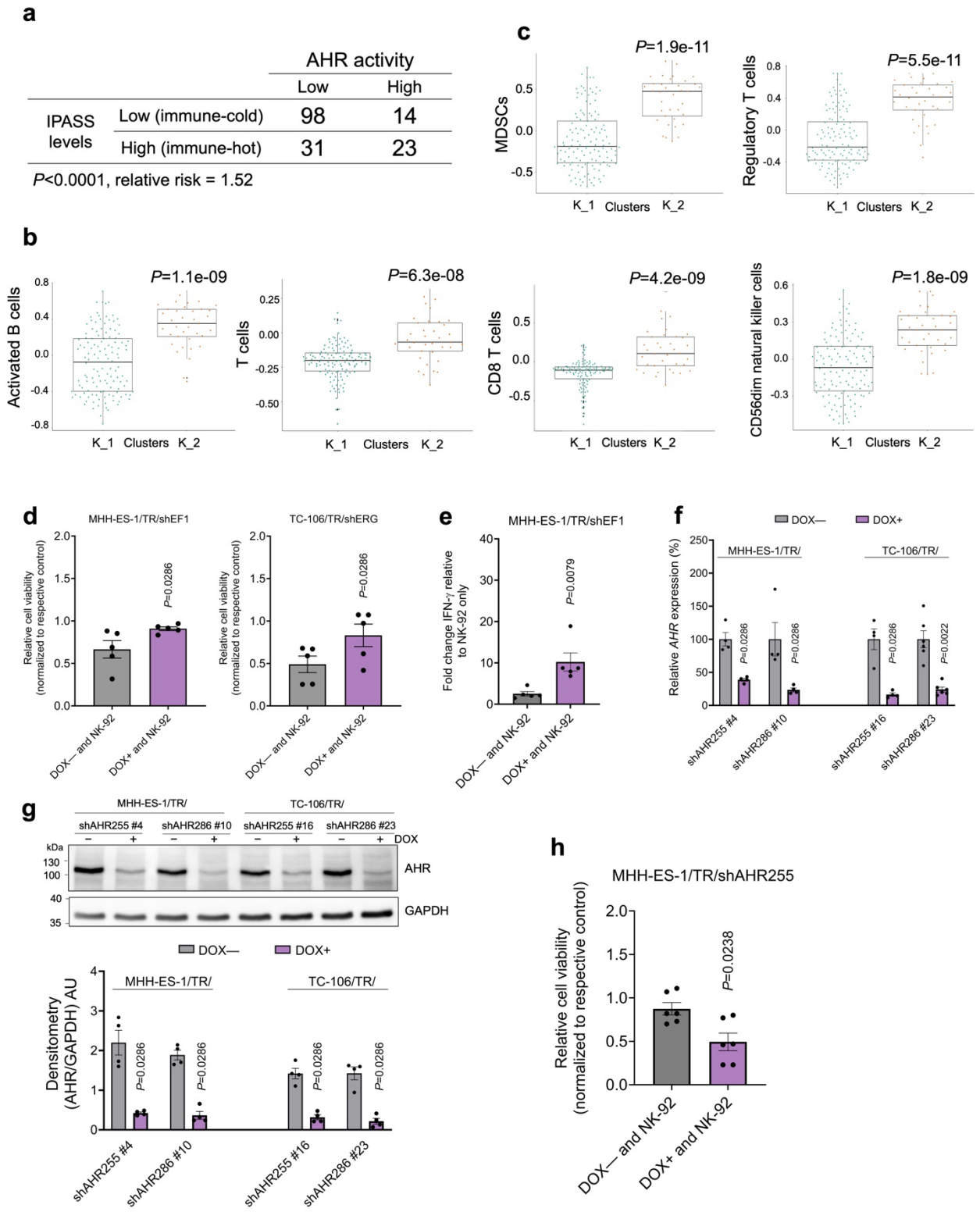

Figure 2. High AHR activity correlates with higher infiltration of immune cells in EwS patients and contributes to an immunoprotective EwS phenotype in *vitro*.

a) Contingency table showing distribution of IPASS score and AHR activity score-based clusters in EwS tumors (n=166). Two-tailed Fisher's exact test. **b)** Comparative analysis of inferred pro-inflammatory immune cell infiltration and **c)** immunosuppressive MDSCs and regulatory T cells infiltration between AHR-low (K1) and -high (K2) activity scoring EwS tumors. Horizontal bars represent the mean and whiskers the SEM. *P*-values were determined by Wilcoxon test. n=166. **d)** Relative cell viability MHH-ES-1/TR/shEF1 and TC-106/TR/shERG and **e)** fold change of interferon (IFN)-γ levels of MHH-ES-1/TR/shEF1 after 24 h co-culture with NK-92 cells. Horizontal bars represent the mean and whiskers the SEM. n=5 independent biological experiments. *P*-values were determined by two-tailed Mann-Whitney test. **f)** Relative *AHR* mRNA and **g**) protein expression after establishing single cell clones with independent DOX-inducible shRNA targeting AHR (255, 286) in MHH-ES-1/TR/ and TC-106/TR/ cells (AU = arbitrary units). n=4–6 biologically

independent experiments. Relative densitometry is shown, calculated from western blots of lysates from n=4 biologically independent experiments. Two-tailed Mann-Whitney test. **h)** Relative cell viability MHH-ES-1/TR/shAHR255 bulk and single clone #4 after 24 h co-culture with NK-92 cells. Horizontal bars represent the mean and whiskers the SEM, n=6 biologically independent experiments. *P*-values were determined by two-tailed Mann-Whitney test.

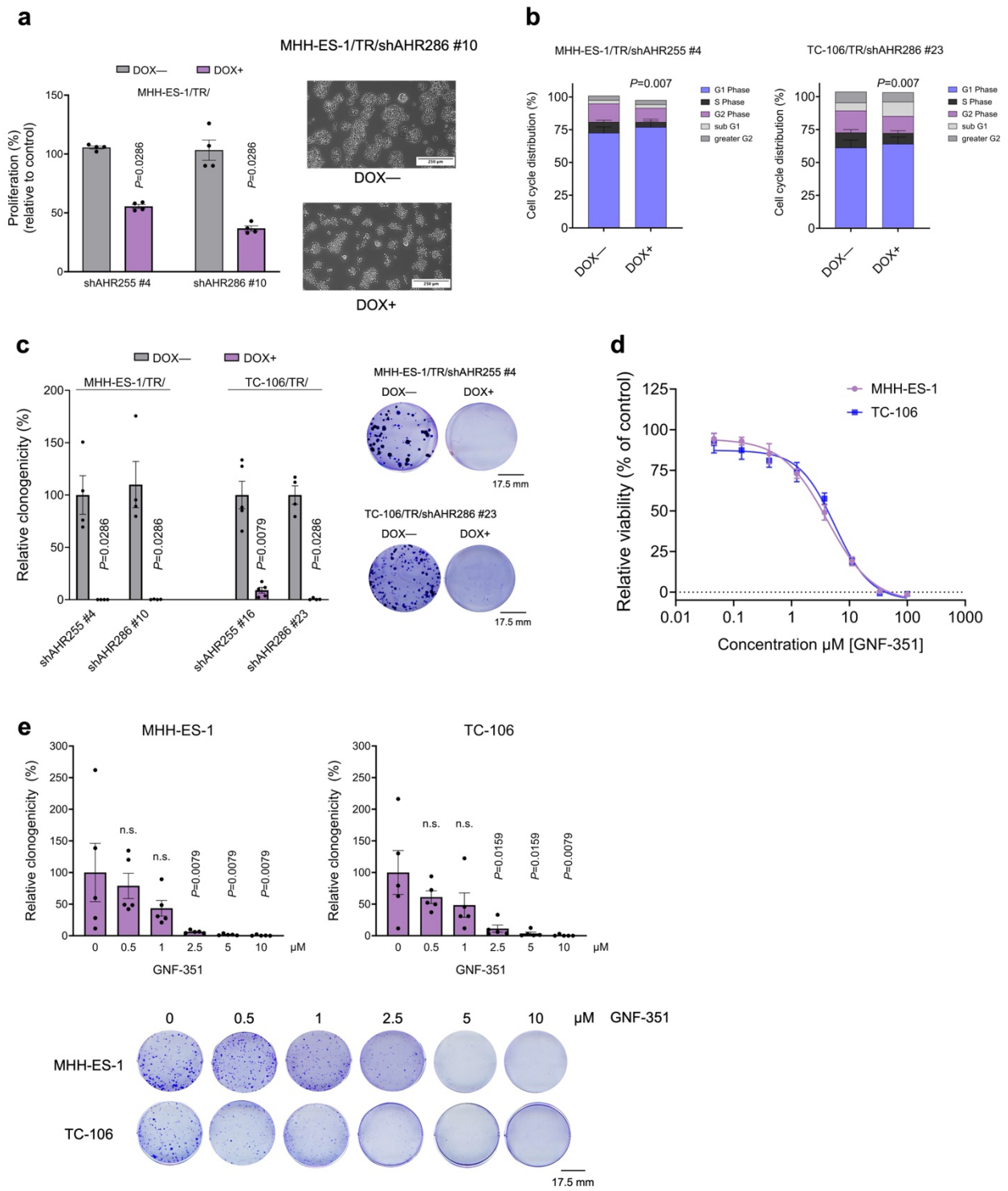

Figure 3. AHR promotes proliferation and clonogenicity of EwS cells *in vitro.*
a) Proliferation of MHH-ES-1/TR/shAHR cells following 96 h of DOX-induced AHR knockdown (left) and representative images of cell proliferation of clone MHH-ES-1/TR/shAHR #10 (5× objective, right). Horizontal bars represent the mean and whiskers the SEM. n=4 biological independent experiments. **b)** Analysis of the cell cycle by PI staining at 96 h post-DOX treatment in MHH-ES-1/TR/shAHR255 #4 cells and TC-106/TR/shAHR286 #23. n=5 biologically independent experiments. *P*-value were calculated from the comparison of the G1 to the S phase with two-tailed Mann-Whitney test. **c)** Relative clonogenicity of single clones MHH-ES-1/TR/shAHR255 #4 and shAHR286 #10 and TC-106/TR/shAHR255 #16 and shAHR286 #23 cells following 10–12 days of DOX-treatment (left) and representative colony images (right). Horizontal bars represent the mean and whiskers the SEM. n=4–5 biologically independent experiments. Two-tailed Mann-Whitney test. **d)** Dose-response curves of MHH-ES-1 and TC-106 cells treated with GNF-351 for 72 h. Relative viability was determined by resazurin assay. n=5 biologically independent experiments. **e)** Relative clonogenicity of MHH-ES-1 and TC-106 cells following 72 h GNF-351 treatment (top) and representative colony images (bottom). n=5 biologically independent experiments. Horizontal bars represent the mean and whiskers the SEM. All comparisons are to the DMSO Ctrl. Two-tailed Mann-Whitney test.

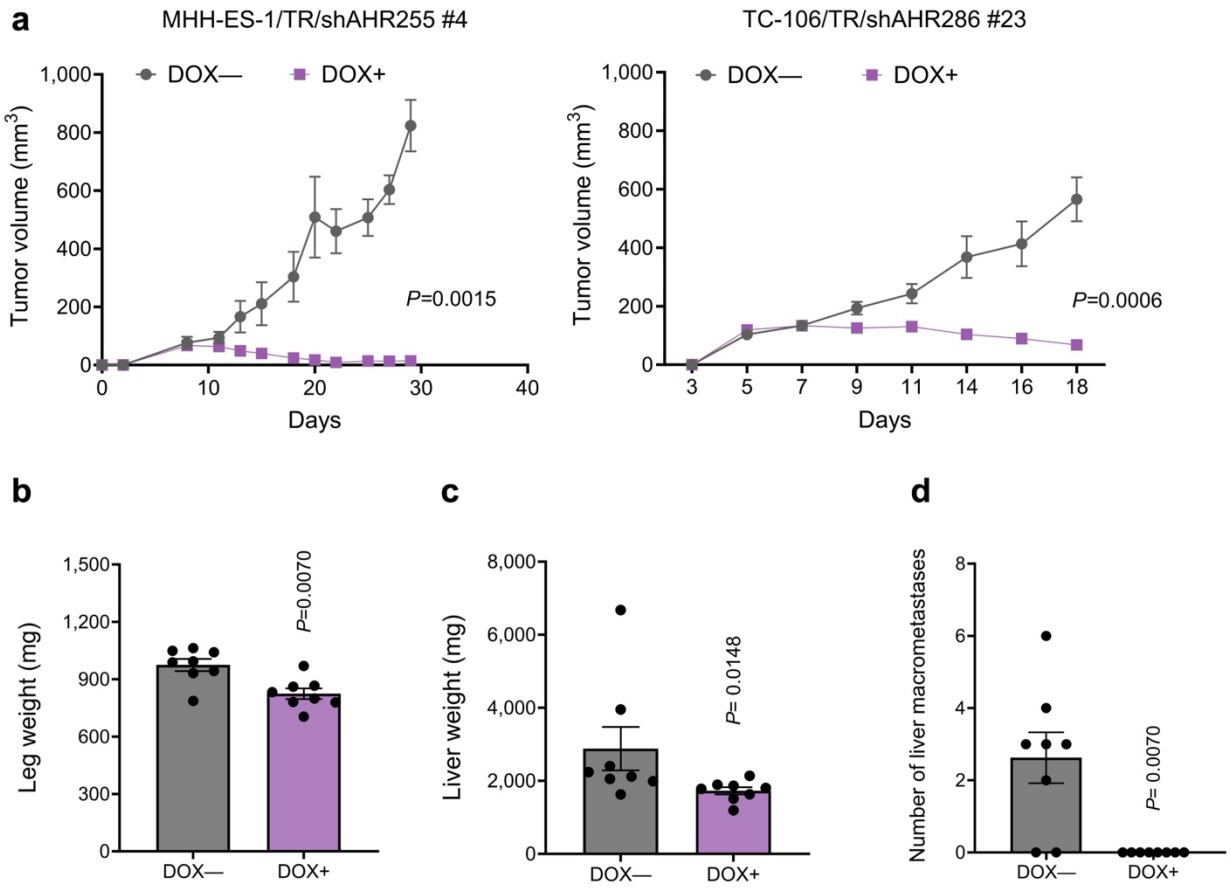

Figure 4. AHR promotes tumor growth and metastasis of EwS *in vivo.*
a) Analysis of tumor volumes (mm^3) over time (days) in two EwS cell lines: MHH-ES-1/TR/shAHR255 #4 and TC-106/TR/shAHR286 #23 with/without DOX-mediated AHR silencing. Horizontal bars represent the mean and whiskers the SEM. n=8 biologically independent animals/conditions. Multigroup unpaired two-tailed Mann-Whitney test. **b)** Leg weight (mg) of both groups at the day of endpoint. **c)** Liver weight (mg) of both groups at the day of the endpoint. d) Number of hepatic macrometastases observed in each mouse. Horizontal bars represent the mean and whiskers the SEM. n=8 biologically independent animals/conditions. Two-tailed Mann-Whitney test.

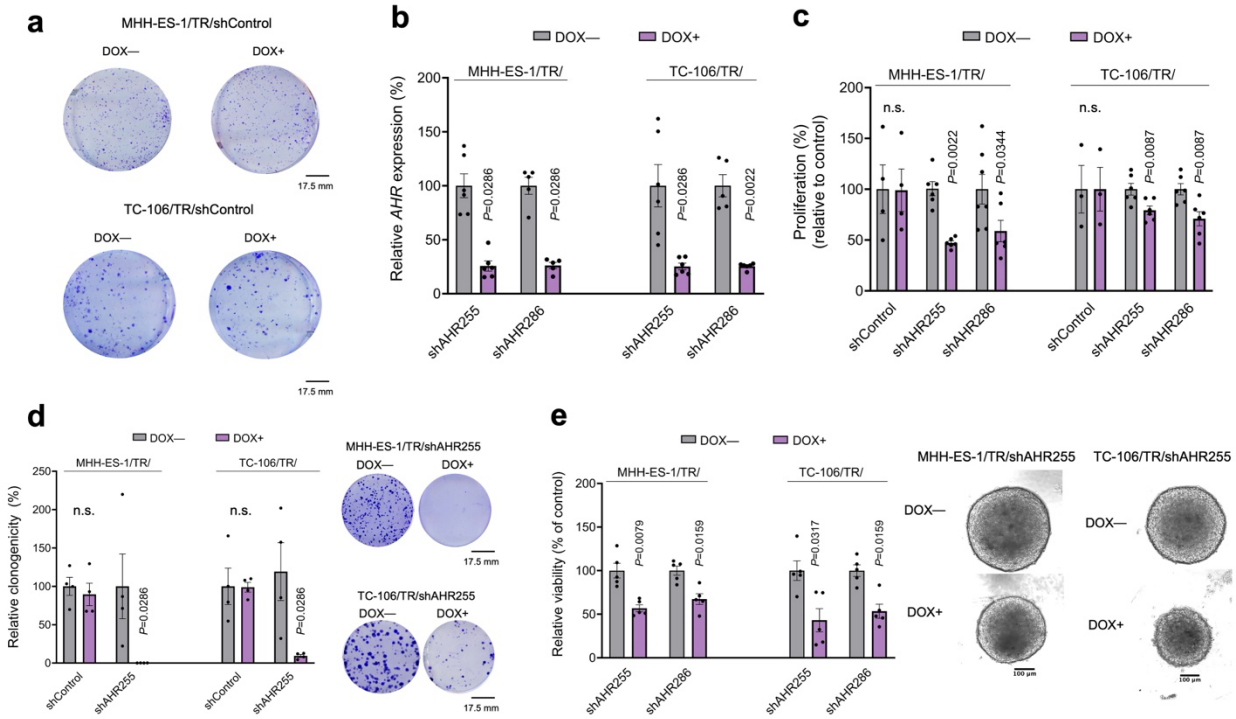

Supplementary Figure 1. Silencing of AHR leads to decreased EwS cell proliferation and clonogenicity.
a) Representative images of colony formation assay in MHH-ES-1/TR/shControl and TC-106/TR/shControl cells following 10–12 days of DOX-treatment. **b)** Relative *AHR* mRNA expression following 96 h DOX treatment in MHH-ES-1/TR/shAHR and TC-106/TR/shAHR cells (bulk level). Horizontal bars represent the mean and whiskers the SEM. n=5–6 biologically independent experiments. Two-tailed Mann-Whitney test. **c)** Proliferation in MHH-ES-1/TR/shAHR and TC-106/TR/shAHR after 96 h of DOX-induced independent shRNAs targeting AHR (255 and 286) or shControls. Counts were performed via trypan blue exclusion method. Horizontal bars represent the mean and whiskers the SEM. n=3–7 biologically independent experiments. Two-tailed Mann-Whitney test. **d)** Relative clonogenicity of MHH-ES-1/TR/shAHR and TC-106/TR/shAHR cells containing a DOX-inducible knockdown construct for targeting AHR (sh255 and 286) and non-targeting control (shControl) for 10–12 days (left) and representative colony images (right). Horizontal bars represent the mean and whiskers the SEM, n=4 biologically independent experiments. Two-tailed Mann-Whitney test. **e)** Relative cell viability of MHH-ES-1/TR/shAHR and TC-106/TR/shAHR (255 and 286) spheroids, as assessed by CellTiterGlo assay, following 96 h treatment with or without DOX (left) and representative images of spheroids (10× objective, right). Horizontal bars represent the mean and whiskers the SEM. n=5 biologically independent experiments. Two-tailed Mann-Whitney test.